

# Extraction of different temperatures and kinetic freeze-out volume in high energy collisions

M. Waqas<sup>1,\*</sup>, G. X. Peng<sup>1,2 †</sup>, Muhammad Ajaz<sup>3 ‡</sup>, Abd Al Karim Haj Ismail<sup>4,5, §</sup>, Z. Wazir<sup>6, ¶</sup>, Li-Li Li<sup>7 ¶</sup>,

<sup>1</sup> *School of Nuclear Science and Technology, University of Chinese Academy of Sciences, Beijing 100049, People's Republic of China,*

<sup>2</sup> *Theoretical Physics Center for Science Facilities, Institute of High Energy Physics, Beijing 100049, China,*

<sup>3</sup> *Department of Physics, Abdul Wali Khan University Mardan, 23200 Mardan, Pakistan,*

<sup>4</sup> *Department of Mathematics and Science, Ajman University, Ajman P.O. Box 346, United Arab Emirates,*

<sup>5</sup> *Nonlinear Dynamics Research Center (NDRC), Ajman University, Ajman P.O. Box 346, United Arab Emirates,*

<sup>6</sup> *Department of physics, Ghazi University, Dera Ghazi Khan, Pakistan,*

<sup>7</sup> *College of Arts and Sciences, Shanxi Agriculture University, Taigu, Shanxi 030801, China.*

**Abstract:** We analyze the transverse momentum ( $p_T$ ) spectra,  $1/N_{ev}[(1/2\pi p_T) d^2N/dydp_T]$ , of kaon, proton, deuteron and triton in different centrality events in gold-gold (Au-Au) collisions at Relativistic Heavy Ion Collisions (RHIC) by Hagedorn thermal model and extracted the excitation function of effective temperature, kinetic freeze-out volume, initial temperature and kinetic freeze-out temperature. We perceived that the effective temperature, initial temperature and kinetic freeze-out temperature sharply increases from 7.7 GeV to 14.5 GeV and then remain static from 14.5-39 GeV, and this consistency may disclose that the onset energy of the phase transition of partial deconfinement and the whole deconfinement are 14.5 and 39 GeV respectively. The kinetic freeze-out volume and mean transverse momentum grows with the rise of collision energy. Furthermore, the different extracted temperatures are observed in the order of time evolution of the interacting system, and they (as well as kinetic freeze-out volume) have an increasing trend from peripheral to central collisions. We also observed the mass dependence of the effective temperature and kinetic freeze-out volume where former increases while the later decreases for heavier particles, which indicates the early freeze-out of the heavier particles.

**Keywords:** effective temperature, initial temperature, kinetic freeze-out temperature, kinetic freeze-out volume, phase transition, onset energy, deconfinement, transverse momentum spectra, high energy collisions.

**PACS:** 12.40.Ee, 13.85.Hd, 25.75.Ag, 25.75.Dw, 24.10.Pa

## 1 Introduction

Temperature is surely one of the most prominent concept in physics due to its wide application in experiments and theoretical analysis. At least four kinds of temperatures are frequently used in the physics of high energy heavy ion collisions which include the initial temperature ( $T_i$ ), chemical freeze-out temperature ( $T_{ch}$ ), kinetic freeze-out temperature or thermal freeze-out temperature ( $T_0$ ) and effective temperature. These temperatures are correspondent to different collision stages.

The excitation degree of interacting system at initial stage of collision is described by the initial temperature and it is the preliminary temperature where hadrons interact both elastically and in-elastically in the hadronic medium. The initial temperature has less studies in the community due to undefined method, though it should be based on the transverse momentum spectra. The initial temperature is followed by the chemical freeze-out temperature which occurs at the stage of chemical freeze-out, when the inelastic collisions cease, where it describes the excitation degree of interacting system at

\*Corresponding author. Email (M. Waqas): waqas\_phy313@yahoo.com, waqas\_phy313@ucas.ac.cn

†Corresponding author. Email (G. X. Peng): gxpeng@ucas.ac.cn, gxpeng@ihep.ac.cn

‡Corresponding author. Email (M. Ajaz): ajaz@awkum.edu.pk, muhammad.ajaz@cern.ch

§Email (A.A.K.H.I): a.hajismail@ajman.ac.ae

¶Email (Z.Wazir): zwazir@gudgk.edu.pk

¶Email (Li-Li Li): shanxi-lll@qq.com

the chemical freeze-out stage. After this stage, no further new particles are produced and the yield of particles become fixed [1–4]. Various thermodynamic models can be used to get the information of this stage in terms of chemical freeze-out temperature and baryon chemical potential [5–8]. Subsequently, the particles experience the elastic collisions only. The inter-particle dissociation grows after further expansion of the system, where the elastic collisions between the particles cease which leads to the kinetic freeze-out stage and there is no longer change in the  $p_T$  spectra after this stage. Various hydrodynamical models can be used to extract the kinetic freeze-out properties [5, 6, 9, 10, 11, 12, 13]. The kinetic freeze-out temperature ( $T_0$ ) and radial flow velocity ( $\beta$ ) characterizes the kinetic freeze-out stage, and it carry the signatures of the transverse expansion of the system. The kinetic freeze-out temperature describes the excitation of interacting system at the kinetic freeze-out stage, and it can be obtained from the transverse momentum spectra of the particles by getting rid of the transverse flow effect and leaving only the contribution of random thermal motion [7, 10, 14–16]. In case, the temperature extracted from  $p_T$  spectra also contains the contribution of transverse flow, this type of temperature is called effective temperature ( $T$ ) [17, 18], which is not a real temperature, but can be obtained from the spectra of heat distribution. The effective temperature occurs at the same time or a little before than kinetic freeze-out temperature. Besides, volume is one of the important parameters to be studied. Different stages correspond to different freeze-out volumes but we are interested in kinetic freeze-out volume. The volume occupied by the hadrons when they decouple from the system is called kinetic freeze-out volume, and it is very important for the extraction of multiplicity, micro-canonical heat capacity and its negative branch or shape of the caloric curves under the thermal constraints [19–23].

Lattice quantum chromodynamics (QCD) is very important in the study of strong interactions and it predicts the transition between the hadronic matter and quark-gluon plasma (QGP) to be a cross-over [24, 25] at  $\mu_B=0$ . Several QCD based models [26–29] and calculations [26] suggest that a system created in collisions corresponding to larger  $\mu_B$ , the phase transition is the first order. In  $T_{ch}-\mu_B$  plane, the point where the first order phase transition ends, is referred as the critical end point (CEP) of QCD [30, 31]. Besides, let consider a certain volume containing baryons. It is quite understandable that baryons have non-zero spatial volume [32]. This clearly indicates that a critical volume

exists where the baryons fill the volume completely and it is assumed that the baryon structure vanishes at the critical volume and forms the quark gluon plasma.

In heavy ion collisions, the production mechanism of light nuclei is a subject of intense debate. In fact, low-energy heavy-ion physics has clearly more connection with nuclear structure physics, for example the studied heavy ions can split up into smaller nuclei that can be scrutinized. Whereas, the collided ions in ultra-relativistic heavy-ion collisions are mainly creating a region of large energy density and temperature that is nearly free of baryon number. e.g. the baryon chemical potential ( $\mu_B$ ) at low energies is about 1 GeV and is close to zero at LHC. This means that the anti-protons and anti-neutrons are equally produced at LHC as their matter counter pieces.  $\mu_B$  is still some MeV at RHIC, which leads to slight variation in the production of protons and anti-protons that results in a small variation of the production of nuclei and anti-nuclei.

In relativistic heavy ion collision, the fundamental mechanism for light nuclei production is not well understood. The light nuclei have small binding energy, therefore they can not persist when the temperature becomes much higher than their binding energy. For light hadrons, the typical kinetic freeze-out temperature is approximately 100 MeV, therefore they may disintegrate and be formed again by coalescence after the decoupling of nucleons.

In this paper we shall study the  $p_T$  spectra of kaon, proton, deuteron and triton in different centrality intervals in Au-Au collisions at various energies at Relativistic Heavy Ion Collision (RHIC). We used the Hagedorn model to extract the effective temperature, initial temperature, kinetic freeze-out temperature, mean transverse momentum, kinetic freeze-out volume by fitting the experimental data of  $p_T$  spectra. Among the above parameters, initial temperature and kinetic freeze-out temperature are extracted by an indirect method which will be discussed in section 3.

## 2 The method and formalism

There are two general processes for the particles production. (1) soft excitation process (2) hard scattering process. Soft process contributes in a narrow  $p_T$  range of 0~2 or 3 GeV/c and is responsible for the production of light flavored particles. Soft excitation has various choices e.g. Hagedorn model [33, 34], blast wave model with Boltzmann Gibbs statistics [10, 35–37], blast wave

model with Tsallis statistics [38–41], Tsallis distribution [42–44] and Standard distribution [45, 46]. Although some particles are produced at not too high energies and are distributed in a wide  $p_T$  range but the contribution of hard scattering can be neglected and the soft excitation is the main contributor for the production of particles. There are limited choices for the hard scattering and can be described by the theory of strong interaction [47–49]. The contribution of hard scattering process is parameterised to an inverse power law [49, 50], i.e Hagedorn function [33, 51]

$$f(p_T) = \frac{1}{N} \frac{dN}{dp_T} = Ap_T \left(1 + \frac{p_T}{p_0}\right)^{-n}, \quad (1)$$

where  $A$  is the normalization constant, and  $p_0$  and  $n$  are the free parameters.

According to [33], the hagedorn model in terms of probability density function at mid-rapidity results in the transverse momentum ( $p_T$ ) spectra distribution as

$$f(p_T) = \frac{1}{N} \frac{dN}{dp_T} = \frac{gV}{(2\pi)^2} p_T \sqrt{p_T^2 + m_0^2} \sum_{n=1}^{\infty} (S)^{n+1} K_1 \left( n \frac{\sqrt{p_T^2 + m_0^2}}{T} \right), \quad (2)$$

where  $N$  is the number of particles,  $g$  is the degeneracy factor,  $V$  is kinetic freeze out volume,  $m_0$  is the rest mass of the particle and  $K$  is the modified Bessel function of second kind.  $S$  can be  $+1$  or  $-1$ .  $S=+1$  is the Fermi system and  $S=-1$  is the Bose system, and  $n$  is the Hagedorn index which is different for different particles, i.e  $n$  can be  $1-5$  for kaon,  $1$  for proton, and for deuteron and triton it is  $1-2$ .  $n$  has no connection with the Fermi or Bose system.

Considering the experimental rapidity range  $[y_{min}, y_{max}]$  around the mid-rapidity, the accurate form of eq.(2) becomes

$$f(p_T) = \frac{1}{N} \frac{dN}{dp_T} = \frac{gV}{(2\pi)^2} p_T \sqrt{p_T^2 + m_0^2} \int_{y_{min}}^{y_{max}} coshy \sum_{n=1}^{\infty} (S)^{n+1} K_1 \left( n \frac{\sqrt{p_T^2 + m_0^2} coshy}{T} \right) dy, \quad (3)$$

Eq. (3) maybe different from Eq.(2). Eq. (3) is more appropriate to the particles produced in a wide  $p_T$  range compared to eq. (2). We can change the rapidity range by adding or subtracting a rapidity shift to cover the mid-rapidity if the rapidity range does not cover the mid-rapidity and thus the contribution of directional movement of the emission source can be excluded.

The single component of Hagedorn model is not enough for the simultaneous description of low  $p_T$  region, so we have used the two-component Hagedorn model in recent work. The Hagedorn model with multi-component can be expressed as

$$f(p_T) = \frac{1}{N} \frac{dN}{dp_T} = \sum_{i=1}^l k_i \frac{gV_i}{(2\pi)^2} p_T \sqrt{p_T^2 + m_0^2} \sum_{n=1}^{\infty} (S)^{n+1} K_1 \left( n \frac{\sqrt{p_T^2 + m_0^2}}{T_i} \right) \quad (4)$$

or

$$f(p_T) = \frac{1}{N} \frac{dN}{dp_T} = \sum_{i=1}^l k_i \frac{gV_i}{(2\pi)^2} p_T \sqrt{p_T^2 + m_0^2} \int_{y_{min}}^{y_{max}} coshy \sum_{n=1}^{\infty} (S)^{n+1} K_1 \left( n \frac{\sqrt{p_T^2 + m_0^2} coshy}{T_i} \right) dy, \quad (5)$$

where  $l$  represents the number of components and  $k_i$  denotes contribution fraction,  $T_i$  is the effective temperature and  $V_i$  is the kinetic freeze out volume corresponding to  $i$ -th component. In case of multi-components, we have used the superposition principle. We would like to clarify that Eq. (2)-(5) are based on both Eq. (2.2) and (B.6) of ref. [33].

$$f(p_T) = \frac{1}{N} \frac{dN}{dp_T} = k f_S(p_T) + (1 - k) f_H(p_T), \quad (6)$$

where  $f_S$  is the soft process with the contribution fraction of  $k$ , and  $f_H$  is the hard components with  $(1 - k)$  contribution fraction. In eq.(5), the soft process contributes from  $0 \sim 2$  or  $3$  GeV/c and hard scattering contributes the whole  $p_T$  region.

We may also use the usual step function in case of two component Hagedorn model

$$f_0(p_T) = A_1 \theta(p_1 - p_T) f_S(p_T) + A_2 \theta(p_T - p_1) f_H(p_T), \quad (7)$$

where  $A_1$  and  $A_2$  are the normalization constants which synthesize  $A_1 f_S(p_1) = A_1 f_H(p_1)$  and  $\theta(x)$  is the usual step function. It should be noted that  $f_S$  and  $f_H$  are just the two components but not the different identified particles.  $T_1$  and  $T_2$  in table 1, 2, 3 and 4 are the soft and hard components respectively.

At the end, we would like to point out that the Hagedorn thermal model is usually associated with continuous mass spectra but we have used the  $p_T$  spectra in the present work. Actually both the  $p_T$  and  $m_T$  spectra can

be inter-convertible, i.e., in order to transform the probability density function  $f_S(p_T)$  of  $p_T$  to the probability density function  $f_{S'}(m_T)$  of  $m_T$ , we have a relation

$$f_S(p_T)|dp_T| = f_{S'}(m_T)|dm_T|, \quad (8)$$

Then

$$f_{S'}(m_T)|dm_T| = \frac{m_T}{\sqrt{m_T^2 - m_0^2}} f_{p_T}(\sqrt{m_T^2 - m_0^2}), \quad (9)$$

### 3 Results and discussion

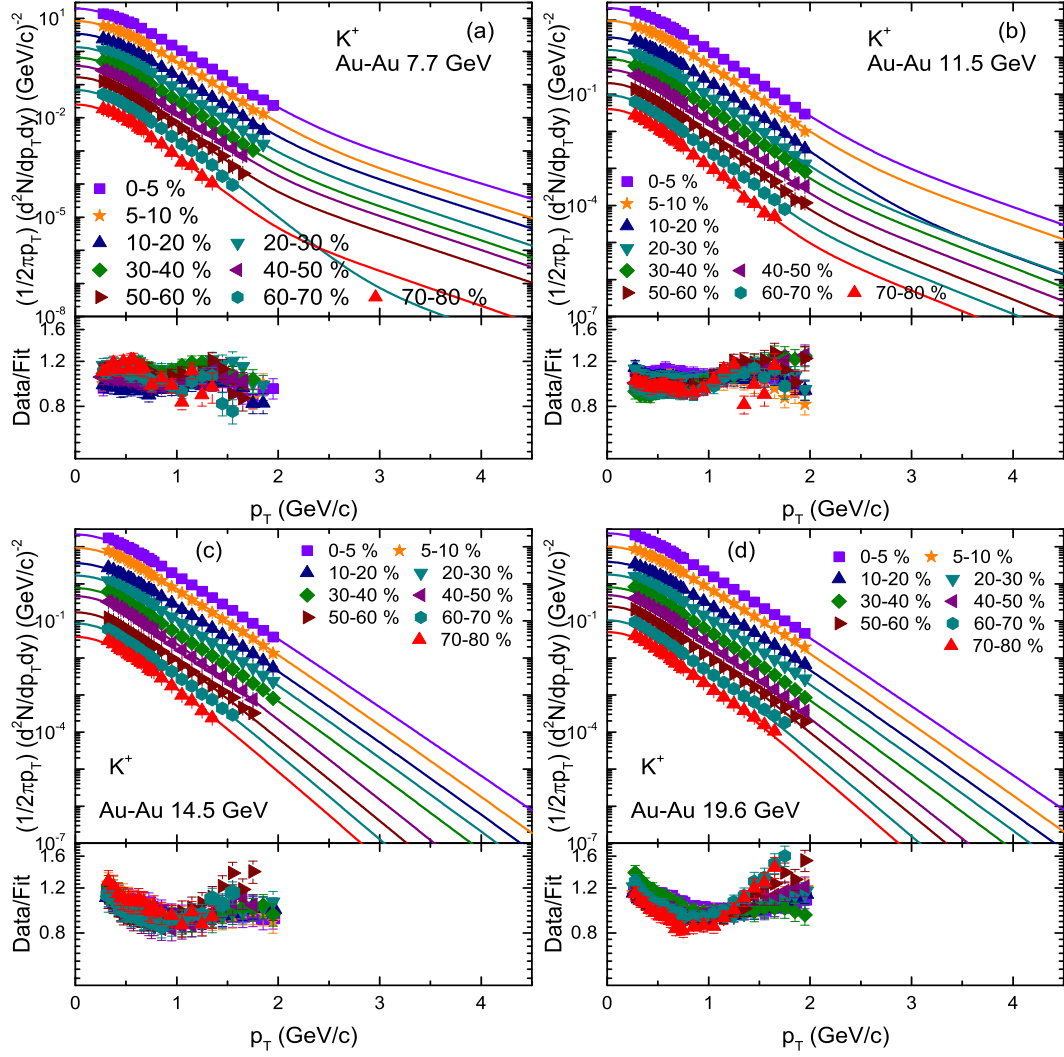
Figure 1 and 2 demonstrate the event centrality dependent double differential transverse momentum ( $p_T$ ) spectra,  $[(1/2\pi p_T) d^2N/dydp_T]$  of  $K^+$  and  $p$  respectively, produced in Au-Au collisions at RHIC-BES. The spectra of  $K^+$  and  $p$  in fig. 1 and 2 respectively from panel (a)-(f) are distributed in to 0–5%, 5–10%, 10–20%, 20–30%, 30–40%, 40–50%, 50–60%, 60–70% and 70–80% centrality bins, while in panel (g) their spectra are distributed in to 0–5%, 5–10%, 10–15%, 15–20%, 20–30%, 30–40%, 40–50%, 50–60%, 60–70%, 70–80% and 80–92% centrality bins. The symbols are the experimental data measured by the STAR Collaboration at  $|y| < 0.1$  [52] in panels (a)-(f) in fig. 1 and 2, and in  $|\eta| < 0.5$  [53] in panel (g) in fig. 1 and 2, and the curves are our fitting results by the Hagedorn thermal model. Each panel is followed by the result of its data/fit ratios to monitor the difference between the data and fit. The results of related parameters along with  $\chi^2$  and degree of freedom (dof) for  $K^+$  and  $p$  respectively, are listed in Table 1 and 2. One can see that the  $p_T$  spectra of  $K^+$  and  $p$  are shown to obey approximately the Hagedorn thermal model.

Figure 3 and 4 are similar to fig.1 and 2, but they present the  $p_T$  spectra of  $d$  and  $t$  produced in Au-Au collisions. The spectra of  $d$  are distributed in 0–10%, 10–20%, 20–40%, 40–60% and 60–80% centrality bins in fig. 3, while the spectra of  $t$  are distributed in 0–10%, 10–20%, 20–40% and 40–80% centrality classes in fig. 4. The symbols are cited from the experimental data measured by the STAR Collaboration at mid-rapidity  $|y| < 0.3$  [54] in fig. 3 and  $|y| < 0.5$  [55] in fig. 4, and the curves are our fitting results by the Hagedorn thermal model. The ratios of data/fit are correspondingly presented in the lower case of each panel. The results of related parameters along with  $\chi^2$  and degree of freedom (dof) for deuteron and triton respectively, are listed in Table 3 and 4. One can see that the  $p_T$  spectra of

deuteron and triton are shown to obey approximately the Hagedorn thermal model.

To study the changing trends of parameters, figure 5 shows the dependence of effective temperature on energy and centrality. Panel (a)-(d) show the results for  $K^+$ ,  $p$ ,  $d$  and  $t$  respectively. Different symbols with different colors represent different centrality bins. The legends presented inside the figure are for the energy range of 7.7-39 GeV, and that of 200 GeV are not included in the figure due to the reason that its centrality intervals are different from the others. The centrality intervals of 200 GeV are given above in fig.1 and 2. The trend of symbols from up to downward shows the dependence of effective temperature on centrality and from left to right shows its dependence on energy. We noticed a significant increase of the effective temperature from 7.7 to 14.5 GeV, and then the trend becomes consistent from 14.5 to 39 GeV, which later on was again increased at maximum energy. We will discuss the behavior of excitation function of  $T$  as that of  $T_0$  later. In addition, the effective temperature is smaller in peripheral collisions and it increases towards central collisions. It is also observed that the effective temperature is increasing with increasing the particles mass, which exhibits a scenario of multiple freeze-out. Larger  $T$  for heavier particles indicate their early freeze-out. One can see that  $t$  ( $K^+$ ) has the largest (lowest) values of  $T$  among the studied particles which means that  $t$  ( $K^+$ ) freeze-out early (later).

Figure 6 is similar to figure 5, but it shows the dependence of kinetic freeze-out volume on energy and centrality. The kinetic freeze-out volume increases with energy due to larger initial bulk system at higher energies. The increase in energy leads to long evolution time which corresponds to larger partonic system and the kinetic freeze-out volume becomes larger in large partonic system. We want to point out that here the initial system is not for the system at evolution time being 0, but at the moment after initial collision, which means that the evolution time is greater than 0, says 1 fm/c for example, for the initial system. The higher the collision energy, the larger the initial system. At present, there is no observation of critical volume but we can study it in future, by analyzing more higher energies and different collision systems containing the production of different particles. In addition, the kinetic freeze-out volume also decreases with decreasing centrality. In fact, there are large number of binary collisions in central collisions due to re-scattering of partons which leads the system quickly to equilibrium state. While when cen-



continue

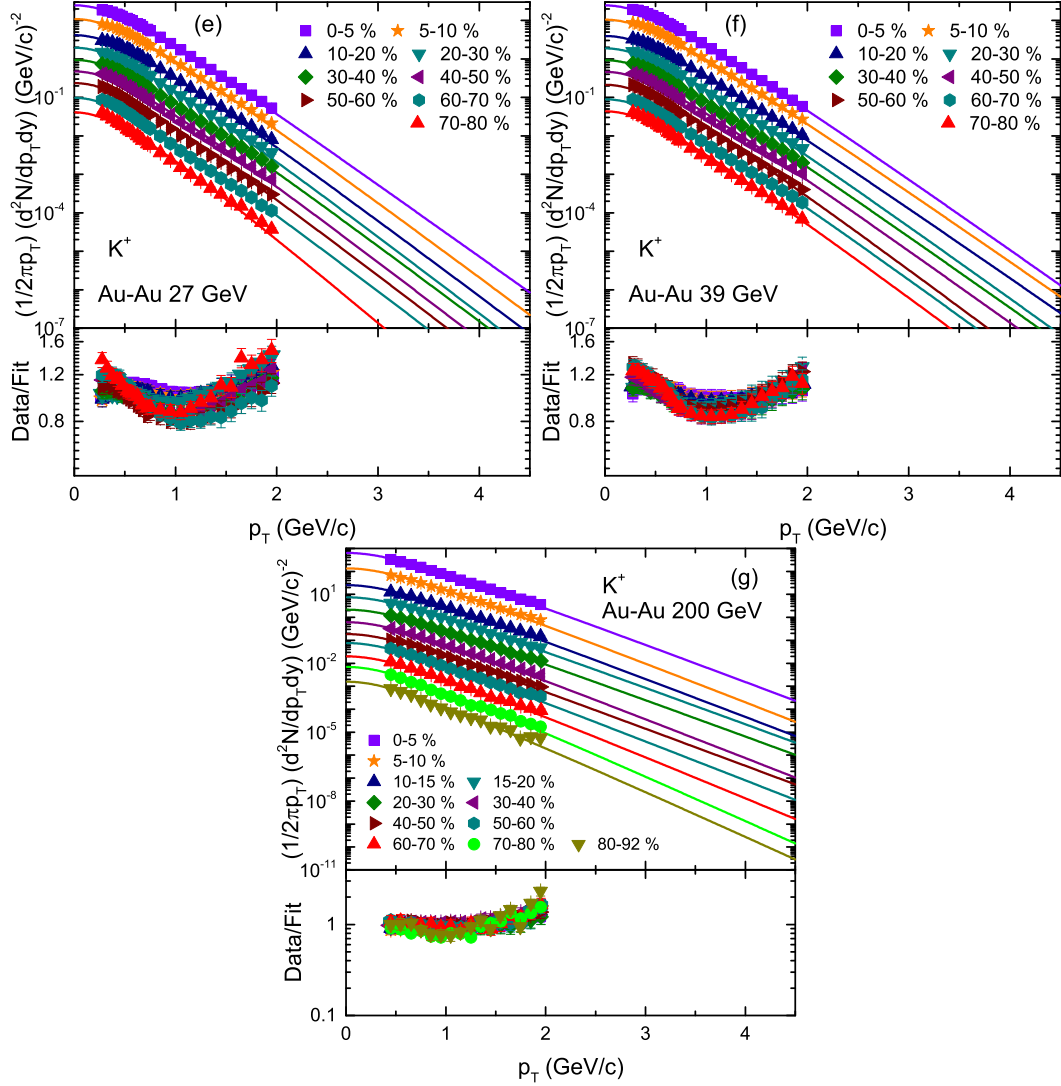
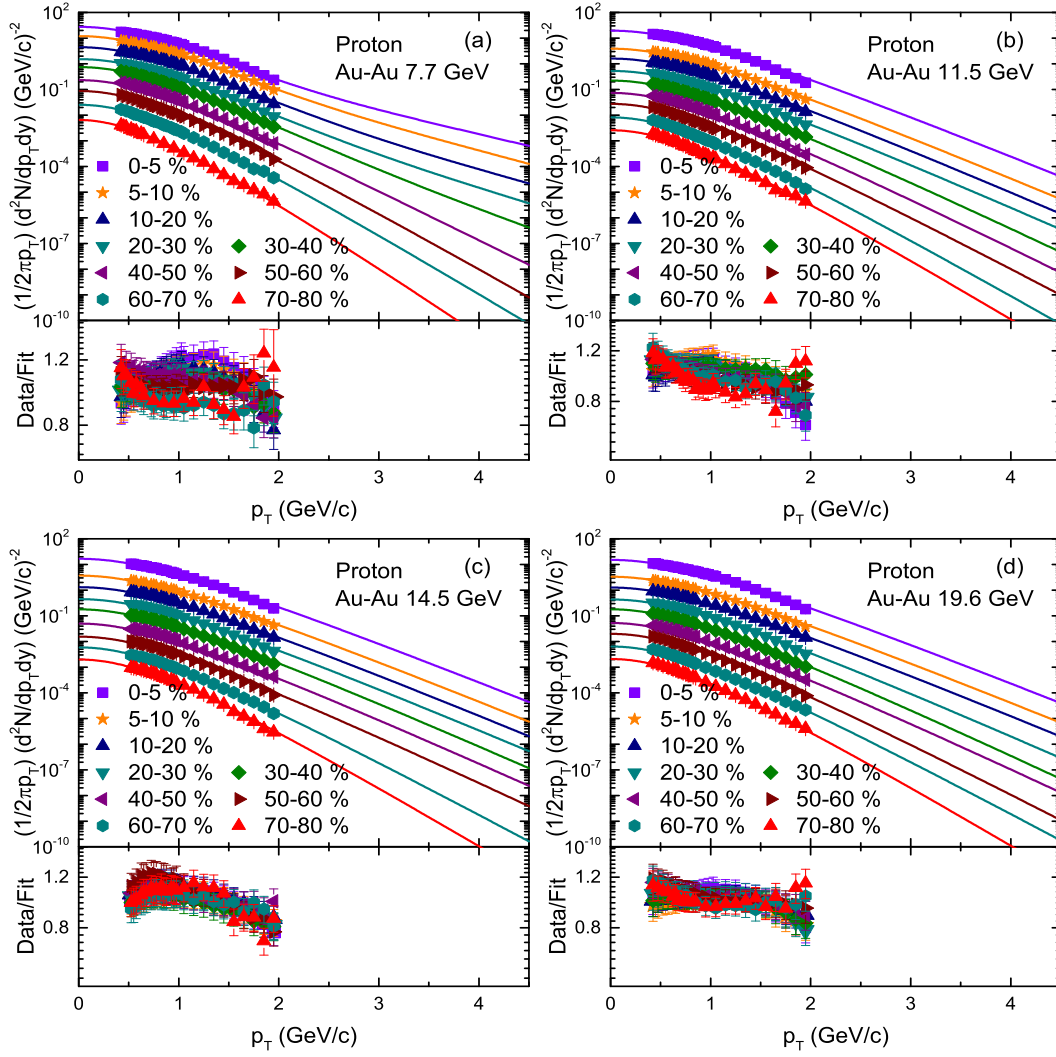


Fig. 1. Transverse momentum spectra of  $K^+$  produced in different centrality intervals in Au-Au collisions. The symbols represent the experimental data measured by STAR Collaboration at RHIC [52, 53], while the curves are our fitting results by using the Hagedorn thermal model. The corresponding ratio of data/fit is presented in each panel. The spectra of  $K^+$  are scaled by in different centrality intervals in order to present the figure clearly. The spectra of  $K^+$  at 7.7-39 GeV in 5–10%, 10–20%, 20–30%, 30–40%, 40–50%, 50–60%, 60–70% and 70–80% centrality bins are scaled by the factor 1/2, 1/4, 1/6, 1/8, 1/10, 1/12, 1/14 and 1/16 respectively, however at 200 GeV the spectra in 5–10%, 10–15%, 15–20%, 20–30%, 30–40%, 40–50%, 50–60%, 60–70%, 70–80% and 80–92% centrality bins are scaled by the factor 1/2, 1/4, 1/6, 1/9, 1/14, 1/25, 1/40, 1/70, 1/120 and 1/230 respectively.



continue

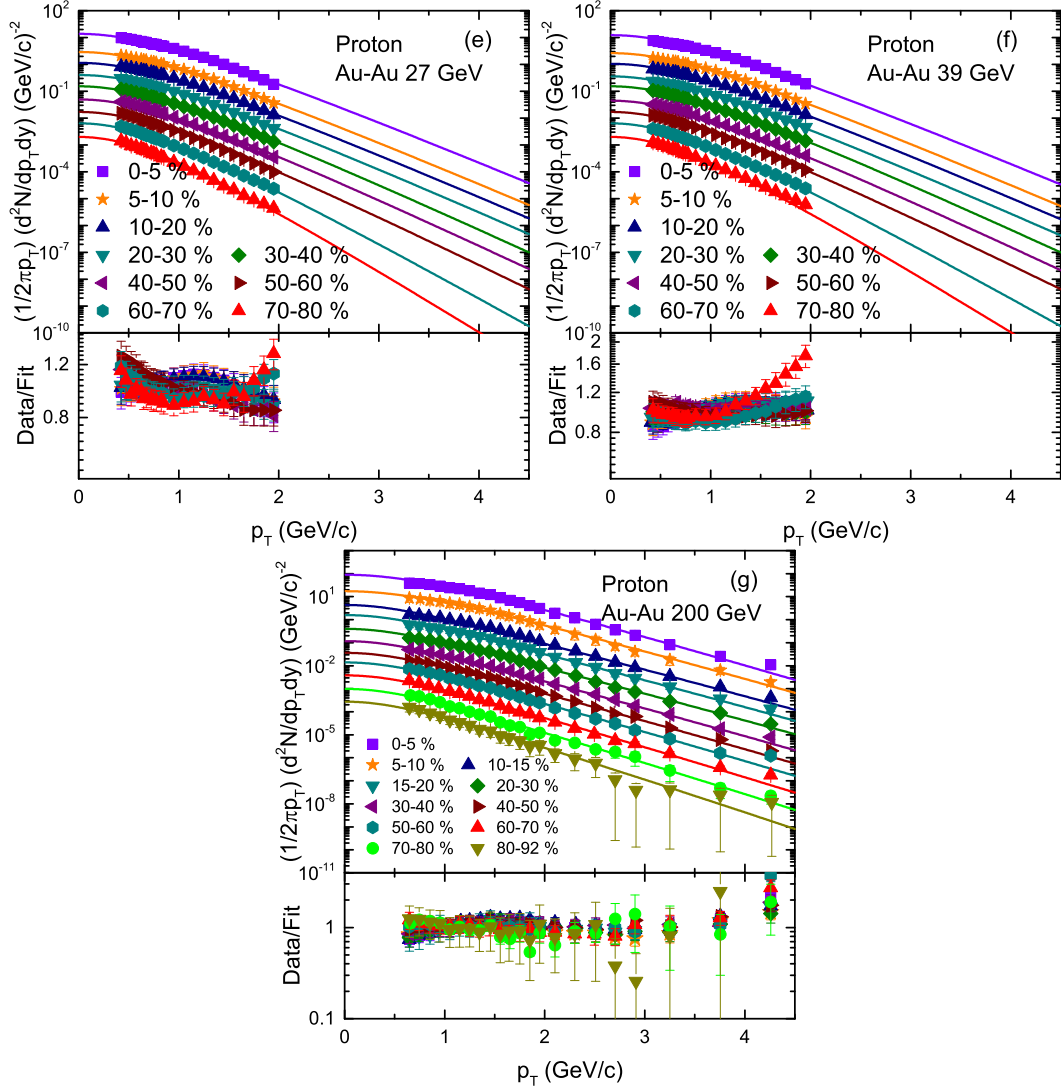
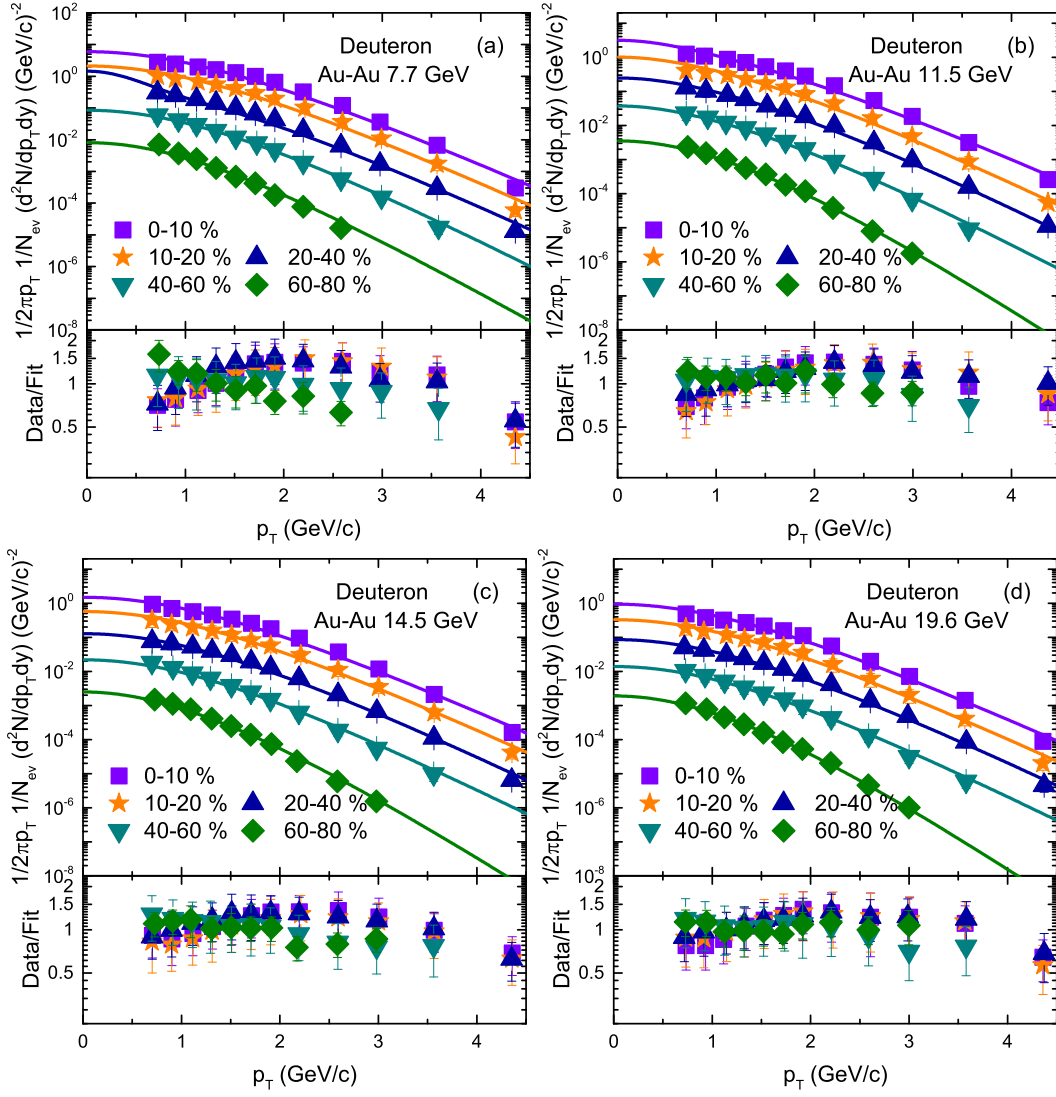


Fig. 2. Transverse momentum spectra of proton produced in different centralities in Au-Au collisions. The symbols represent the experimental data measured by STAR Collaboration at RHIC [52, 53], while the curves are our fitting results by using the Hagedorn thermal model. The corresponding ratio of data/fit is presented in each panel. The spectra of  $p$  at 7.7 GeV in 5–10%, 10–20%, 20–30%, 30–40%, 40–50%, 50–60%, 60–70% and 70–80% centrality bins are scaled by the factor  $1/2$ ,  $1/4$ ,  $1/8$ ,  $1/12$ ,  $1/22$ ,  $1/40$ ,  $1/80$  and  $1/180$  respectively, and the spectra at 11.5–39 GeV in 5–10%, 10–20%, 20–30%, 30–40%, 40–50%, 50–60%, 60–70% and 70–80% centrality bins are scaled by the factor  $1/4$ ,  $1/8$ ,  $1/16$ ,  $1/28$ ,  $1/55$ ,  $1/90$ ,  $1/160$  and  $1/270$ , however at 200 GeV the spectra in 5–10%, 10–15%, 15–20%, 20–30%, 30–40%, 40–50%, 50–60%, 60–70%, 70–80% and 80–92% centrality bins are scaled by the factor  $1/2$ ,  $1/4$ ,  $1/6$ ,  $1/9$ ,  $1/14$ ,  $1/25$ ,  $1/40$ ,  $1/70$ ,  $1/120$  and  $1/230$  respectively.





continue

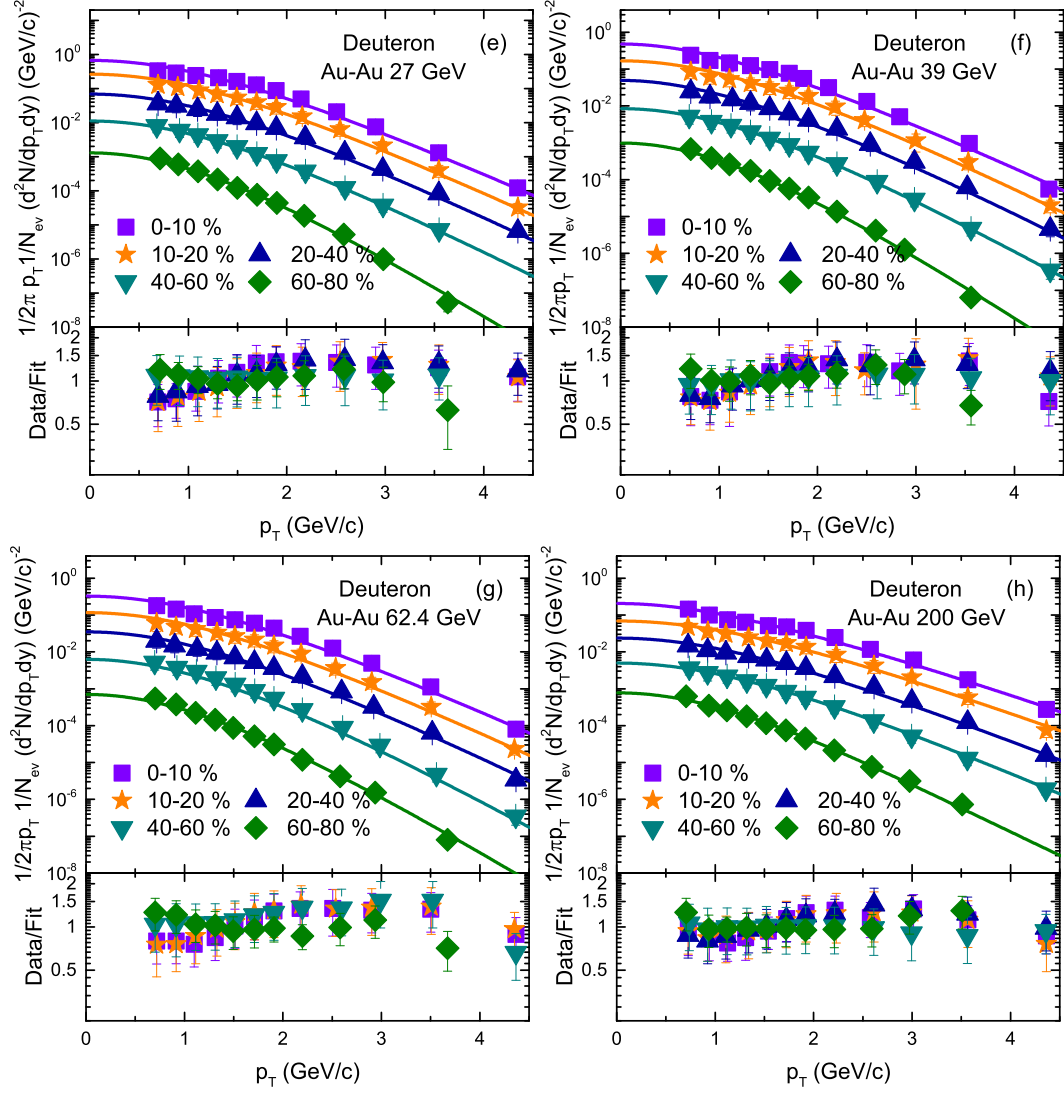
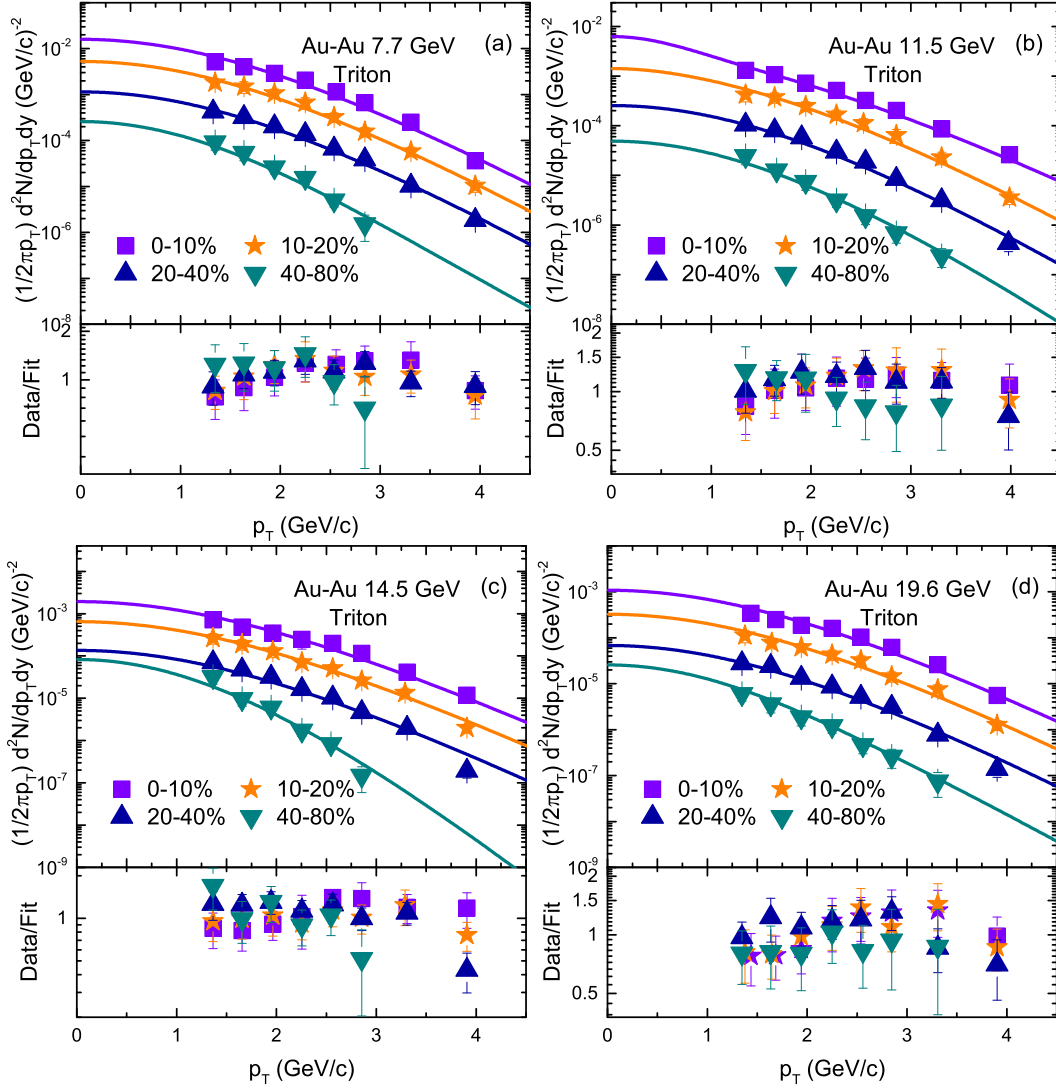


Fig. 3. Transverse momentum spectra of deuteron produced in different centralities in Au-Au collisions at mid-rapidity  $|y| < 0.3$  [54]. The symbols represent the experimental data measured by STAR Collaboration at RHIC, while the curves are our fitted results by using the Hagedorn thermal model. The corresponding ratio of data/fit is presented in each panel.



continue

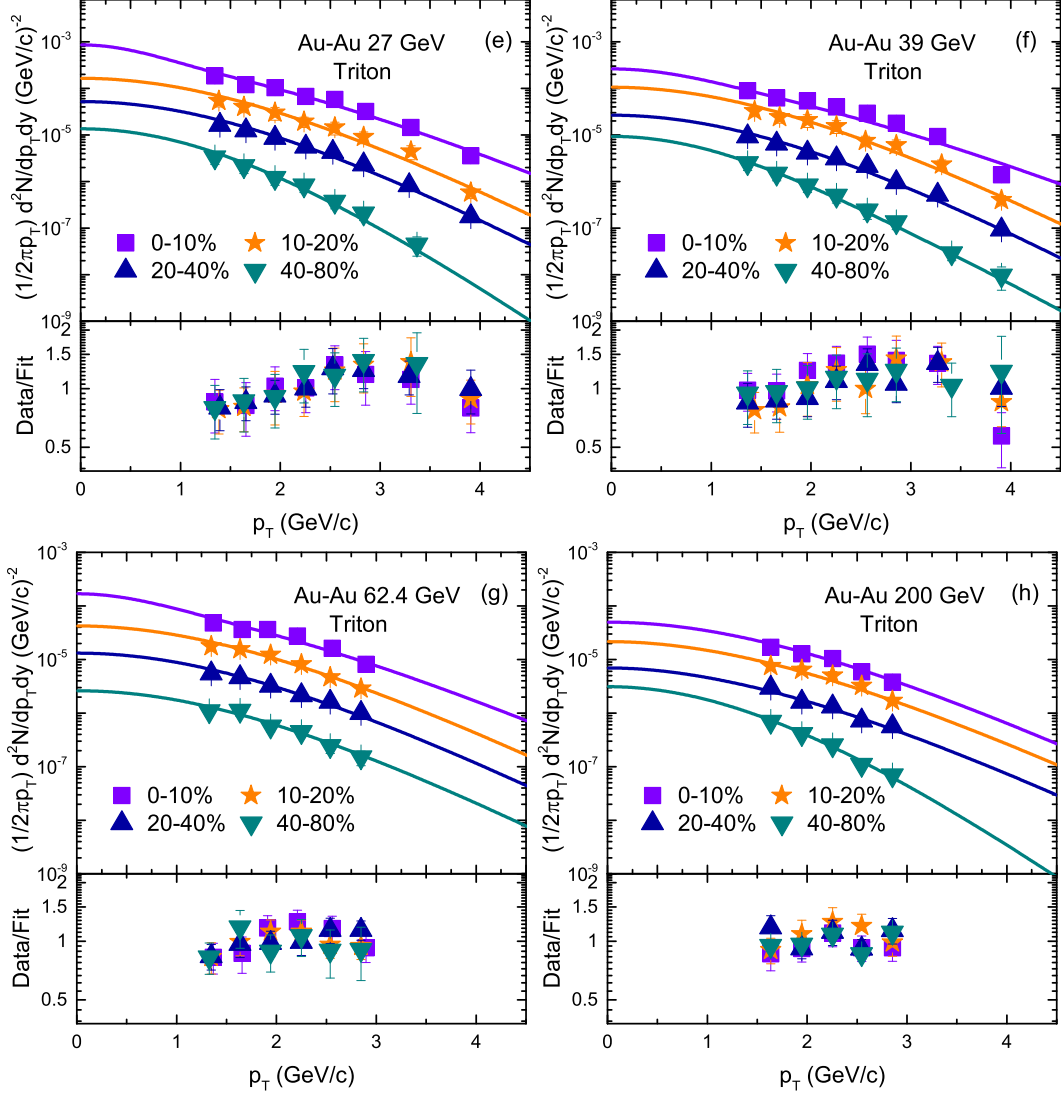


Fig. 4. Transverse momentum spectra of triton produced in different centralities in Au-Au collisions at mid-rapidity  $|y| < 0.3$  [55]. The symbols represent the experimental data measured by STAR Collaboration at RHIC, while the curves are our fitted results by using the Hagedorn thermal model. The corresponding ratio of data/fit is presented in each panel.

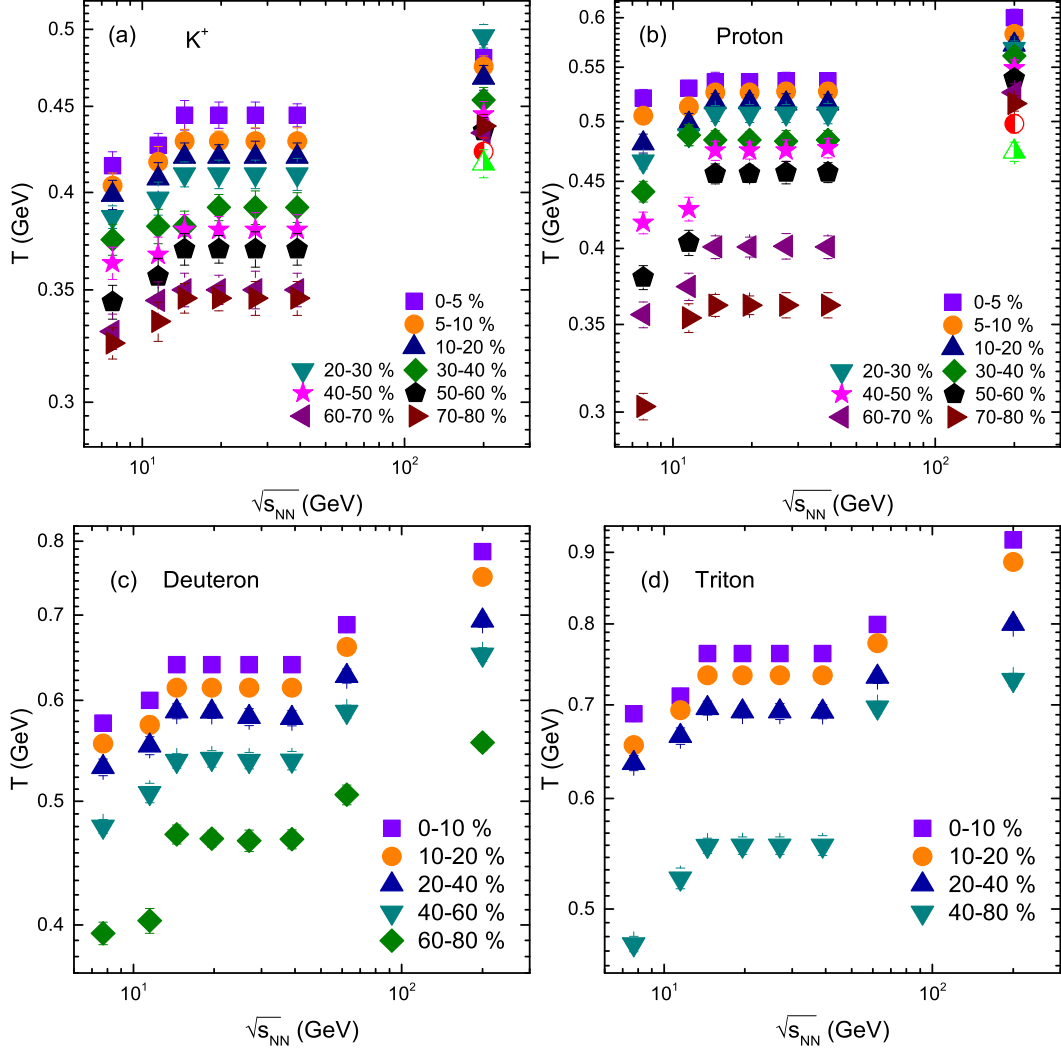


Fig. 5. Dependence of effective temperature on energy and centrality for  $K^+$ ,  $p$ ,  $d$  and  $t$ . The centrality bins at the center of mass energy from 7.7-39 GeV are same and they shown in each panel, while the centrality bins at 200 GeV are different and are not presented because the figure will be much crowded.

Table 1. Values of free parameters ( $T_1$ ,  $T_2$ ,  $\mathcal{E} \rightarrow V_1$ ,  $V_2$  and  $k$ ), normalization constant ( $N_0$ ),  $\chi^2$ , and degree of freedom (dof) corresponding to the curves in Fig. 1.

Collisions	Centrality	$T_1$ (GeV)	$T_2$ (GeV)	$V_1(fm^3)$	$V_2(fm^3)$	$k$	$N_0$	$\chi^2/\text{dof}$
Fig. 1 Au-Au 7.7 GeV	0-5%	$0.414 \pm 0.009$	$0.895 \pm 0.008$	$3600 \pm 210$	$2430 \pm 190$	$0.97 \pm 0.19$	$1.2 \pm 0.04$	4/22
	5-10%	$0.390 \pm 0.008$	$0.845 \pm 0.008$	$3500 \pm 170$	$2350 \pm 200$	$0.97 \pm 0.18$	$0.5 \pm 0.03$	7/22
	10-20%	$0.380 \pm 0.007$	$0.845 \pm 0.008$	$3500 \pm 160$	$2150 \pm 100$	$0.96 \pm 0.20$	$0.20 \pm 0.03$	17/22
	20-30%	$0.367 \pm 0.008$	$0.805 \pm 0.008$	$3300 \pm 168$	$2136 \pm 188$	$0.955 \pm 0.16$	$0.08 \pm 0.004$	10/22
	30-40%	$0.357 \pm 0.006$	$0.805 \pm 0.007$	$3100 \pm 174$	$2136 \pm 140$	$0.96 \pm 0.20$	$0.04 \pm 0.004$	16/21
	40-50%	$0.345 \pm 0.007$	$0.802 \pm 0.007$	$3000 \pm 171$	$2036 \pm 160$	$0.96 \pm 0.14$	$0.022 \pm 0.004$	7/20
	50-60%	$0.330 \pm 0.008$	$0.800 \pm 0.008$	$2800 \pm 149$	$2036 \pm 140$	$0.97 \pm 0.16$	$0.01 \pm 0.003$	13/19
	60-70%	$0.330 \pm 0.009$	$0.800 \pm 0.007$	$2808 \pm 156$	$1823 \pm 190$	$0.999 \pm 0.19$	$0.004 \pm 0.0004$	10/18
Fig. 1 Au-Au 11.5 GeV	70-80%	$0.316 \pm 0.008$	$0.780 \pm 0.008$	$2808 \pm 170$	$1623 \pm 154$	$0.98 \pm 0.18$	$0.00144 \pm 0.0003$	8/15
	0-5%	$0.413 \pm 0.007$	$0.869 \pm 0.006$	$3900 \pm 208$	$2230 \pm 170$	$0.97 \pm 0.12$	$6.25 \pm 0.6$	12/22
	5-10%	$0.403 \pm 0.006$	$0.869 \pm 0.007$	$3900 \pm 190$	$2230 \pm 160$	$0.97 \pm 0.16$	$0.55 \pm 0.05$	4/23
	10-20%	$0.403 \pm 0.007$	$0.861 \pm 0.006$	$3700 \pm 190$	$2230 \pm 160$	$0.99 \pm 0.17$	$0.20 \pm 0.05$	6/23
	20-30%	$0.383 \pm 0.009$	$0.840 \pm 0.006$	$3600 \pm 181$	$2100 \pm 181$	$0.97 \pm 0.15$	$0.09 \pm 0.003$	8/23
	30-40%	$0.363 \pm 0.009$	$0.780 \pm 0.005$	$3500 \pm 193$	$2000 \pm 170$	$0.955 \pm 0.21$	$0.05 \pm 0.003$	18/23
	40-50%	$0.350 \pm 0.006$	$0.780 \pm 0.008$	$3400 \pm 169$	$1900 \pm 176$	$0.96 \pm 0.10$	$0.025 \pm 0.005$	12/23
	50-60%	$0.340 \pm 0.006$	$0.780 \pm 0.005$	$3200 \pm 163$	$1900 \pm 163$	$0.96 \pm 0.14$	$0.011 \pm 0.003$	11/23
Fig. 1 Au-Au 14.5 GeV	60-70%	$0.328 \pm 0.008$	$0.750 \pm 0.006$	$3200 \pm 169$	$1900 \pm 170$	$0.96 \pm 0.11$	$0.005 \pm 0.0004$	15/23
	70-80%	$0.318 \pm 0.006$	$0.745 \pm 0.007$	$3551 \pm 150$	$1700 \pm 103$	$0.96 \pm 0.10$	$0.002 \pm 0.0004$	6/23
	0-5%	$0.429 \pm 0.009$	$0.469 \pm 0.007$	$4200 \pm 209$	$2430 \pm 140$	$0.61 \pm 0.11$	$1.5 \pm 0.2$	3/23
	5-10%	$0.434 \pm 0.008$	$0.420 \pm 0.006$	$4200 \pm 190$	$2200 \pm 110$	$0.62 \pm 0.13$	$0.65 \pm 0.05$	4/23
	10-20%	$0.429 \pm 0.009$	$0.420 \pm 0.008$	$4200 \pm 150$	$2000 \pm 120$	$0.61 \pm 0.08$	$0.25 \pm 0.04$	3/23
	20-30%	$0.420 \pm 0.006$	$0.420 \pm 0.007$	$4000 \pm 119$	$2000 \pm 103$	$0.60 \pm 0.05$	$0.12 \pm 0.03$	18/23
	30-40%	$0.410 \pm 0.007$	$0.410 \pm 0.006$	$3800 \pm 160$	$2000 \pm 110$	$0.62 \pm 0.07$	$0.07 \pm 0.004$	16/23
	40-50%	$0.370 \pm 0.008$	$0.400 \pm 0.007$	$3800 \pm 162$	$1800 \pm 123$	$0.62 \pm 0.08$	$0.03 \pm 0.003$	11/23
Fig. 1 Au-Au 19.6 GeV	50-60%	$0.370 \pm 0.008$	$0.370 \pm 0.007$	$3600 \pm 160$	$1620 \pm 103$	$0.62 \pm 0.04$	$0.011 \pm 0.003$	10/23
	60-70%	$0.360 \pm 0.006$	$0.350 \pm 0.008$	$3600 \pm 166$	$1620 \pm 100$	$0.62 \pm 0.14$	$0.005 \pm 0.0004$	6/23
	70-80%	$0.350 \pm 0.006$	$0.346 \pm 0.006$	$3400 \pm 150$	$1620 \pm 103$	$0.62 \pm 0.10$	$0.0024 \pm 0.0004$	9/23
	0-5%	$0.429 \pm 0.007$	$0.469 \pm 0.006$	$4600 \pm 220$	$2430 \pm 150$	$0.61 \pm 0.11$	$1.5 \pm 0.2$	14/23
	5-10%	$0.434 \pm 0.005$	$0.420 \pm 0.005$	$4300 \pm 200$	$2430 \pm 119$	$0.62 \pm 0.10$	$0.65 \pm 0.05$	9/23
	10-20%	$0.429 \pm 0.006$	$0.420 \pm 0.008$	$4640 \pm 178$	$2430 \pm 100$	$0.61 \pm 0.09$	$0.25 \pm 0.04$	13/23
	20-30%	$0.420 \pm 0.006$	$0.420 \pm 0.008$	$4200 \pm 175$	$2200 \pm 118$	$0.60 \pm 0.08$	$0.12 \pm 0.03$	5/23
	30-40%	$0.410 \pm 0.006$	$0.410 \pm 0.006$	$4000 \pm 180$	$2225 \pm 132$	$0.62 \pm 0.07$	$0.07 \pm 0.004$	16/23
Fig. 1 Au-Au 27 GeV	40-50%	$0.370 \pm 0.009$	$0.400 \pm 0.006$	$3930 \pm 162$	$2100 \pm 133$	$0.62 \pm 0.08$	$0.03 \pm 0.003$	12/23
	50-60%	$0.370 \pm 0.008$	$0.370 \pm 0.006$	$4000 \pm 150$	$1800 \pm 116$	$0.62 \pm 0.06$	$0.011 \pm 0.003$	4/23
	60-70%	$0.360 \pm 0.006$	$0.350 \pm 0.006$	$3700 \pm 160$	$1920 \pm 110$	$0.62 \pm 0.10$	$0.005 \pm 0.0004$	19/23
	70-80%	$0.350 \pm 0.006$	$0.346 \pm 0.006$	$3700 \pm 150$	$1670 \pm 106$	$0.62 \pm 0.08$	$0.0024 \pm 0.0005$	11/23
	0-5%	$0.542 \pm 0.009$	$0.230 \pm 0.009$	$4900 \pm 220$	$2630 \pm 150$	$0.985 \pm 0.13$	$1.9 \pm 0.3$	11/20
	5-10%	$0.529 \pm 0.007$	$0.221 \pm 0.006$	$4700 \pm 200$	$2630 \pm 119$	$0.993 \pm 0.05$	$1.7 \pm 0.2$	10/23
	10-20%	$0.522 \pm 0.008$	$0.210 \pm 0.008$	$4600 \pm 178$	$2530 \pm 100$	$0.98 \pm 0.08$	$1.3 \pm 0.4$	8/20
	20-30%	$0.510 \pm 0.006$	$0.200 \pm 0.006$	$4400 \pm 175$	$2530 \pm 118$	$0.99 \pm 0.09$	$0.9 \pm 0.04$	4/20
Fig. 1 Au-Au 39 GeV	30-40%	$0.490 \pm 0.008$	$0.180 \pm 0.007$	$4200 \pm 180$	$2530 \pm 132$	$0.98 \pm 0.11$	$0.6 \pm 0.03$	8/20
	40-50%	$0.478 \pm 0.009$	$0.160 \pm 0.009$	$4000 \pm 162$	$2500 \pm 133$	$0.99 \pm 0.08$	$0.4 \pm 0.03$	14/20
	50-60%	$0.460 \pm 0.007$	$0.150 \pm 0.007$	$4000 \pm 150$	$2300 \pm 116$	$0.99 \pm 0.10$	$0.22 \pm 0.03$	20/20
	60-70%	$0.404 \pm 0.006$	$0.150 \pm 0.008$	$4000 \pm 160$	$2100 \pm 110$	$0.99 \pm 0.12$	$0.13 \pm 0.04$	11/20
	70-80%	$0.364 \pm 0.008$	$0.160 \pm 0.008$	$3900 \pm 150$	$2000 \pm 106$	$0.99 \pm 0.09$	$0.065 \pm 0.005$	19/20
	0-5%	$0.542 \pm 0.005$	$0.230 \pm 0.006$	$5300 \pm 260$	$2490 \pm 100$	$0.985 \pm 0.06$	$1.7 \pm 0.22$	14/19
	5-10%	$0.529 \pm 0.005$	$0.221 \pm 0.005$	$5300 \pm 210$	$2290 \pm 110$	$0.993 \pm 0.07$	$1.5 \pm 0.23$	11/19
	10-20%	$0.522 \pm 0.007$	$0.210 \pm 0.007$	$5100 \pm 160$	$2290 \pm 110$	$0.98 \pm 0.08$	$1.2 \pm 0.18$	10/19
Fig. 1 Au-Au 200 GeV	20-30%	$0.510 \pm 0.006$	$0.200 \pm 0.007$	$5000 \pm 170$	$2200 \pm 123$	$0.99 \pm 0.11$	$0.8 \pm 0.04$	10/19
	30-40%	$0.490 \pm 0.008$	$0.180 \pm 0.006$	$5000 \pm 200$	$2000 \pm 121$	$0.98 \pm 0.04$	$0.6 \pm 0.03$	7/19
	40-50%	$0.480 \pm 0.005$	$0.160 \pm 0.008$	$4820 \pm 174$	$2000 \pm 150$	$0.99 \pm 0.09$	$0.36 \pm 0.04$	1/19
	50-60%	$0.460 \pm 0.007$	$0.150 \pm 0.006$	$4800 \pm 180$	$1800 \pm 100$	$0.99 \pm 0.06$	$0.22 \pm 0.023$	5.5/19
	60-70%	$0.404 \pm 0.008$	$0.150 \pm 0.006$	$4600 \pm 160$	$1800 \pm 107$	$0.99 \pm 0.13$	$0.13 \pm 0.024$	19/19
	70-80%	$0.364 \pm 0.008$	$0.150 \pm 0.006$	$4300 \pm 199$	$1800 \pm 130$	$0.99 \pm 0.08$	$0.065 \pm 0.0022$	24/19
	0-5%	$0.602 \pm 0.007$	$0.430 \pm 0.006$	$5700 \pm 240$	$2900 \pm 130$	$0.999 \pm 0.06$	$13 \pm 1.3$	23/19
	5-10%	$0.590 \pm 0.007$	$0.430 \pm 0.006$	$5200 \pm 200$	$3200 \pm 130$	$0.96 \pm 0.08$	$6 \pm 0.4$	21/19
	10-15%	$0.697 \pm 0.006$	$0.413 \pm 0.006$	$5300 \pm 190$	$2900 \pm 130$	$0.56 \pm 0.05$	$2.5 \pm 0.3$	13/19
	15-20%	$0.690 \pm 0.008$	$0.413 \pm 0.007$	$5300 \pm 180$	$2700 \pm 135$	$0.56 \pm 0.09$	$1.4 \pm 0.3$	10/19
	20-30%	$0.680 \pm 0.009$	$0.410 \pm 0.006$	$4900 \pm 200$	$2800 \pm 128$	$0.56 \pm 0.06$	$0.55 \pm 0.04$	9/19
	30-40%	$0.689 \pm 0.009$	$0.413 \pm 0.007$	$4800 \pm 174$	$2730 \pm 150$	$0.53 \pm 0.10$	$0.25 \pm 0.04$	8/19
	40-50%	$0.660 \pm 0.009$	$0.404 \pm 0.008$	$4600 \pm 180$	$2730 \pm 140$	$0.53 \pm 0.11$	$0.14 \pm 0.02$	15/19
	50-60%	$0.640 \pm 0.008$	$0.402 \pm 0.007$	$4400 \pm 160$	$2700 \pm 137$	$0.52 \pm 0.12$	$0.09 \pm 0.004$	10/19
	60-70%	$0.620 \pm 0.008$	$0.404 \pm 0.008$	$4560 \pm 199$	$2400 \pm 138$	$0.52 \pm 0.08$	$0.043 \pm 0.005$	9/19
	70-80%	$0.600 \pm 0.006$	$0.389 \pm 0.009$	$4300 \pm 160$	$2400 \pm 126$	$0.52 \pm 0.10$	$0.019 \pm 0.004$	14/19
	80-92%	$0.570 \pm 0.008$	$0.370 \pm 0.007$	$4000 \pm 199$	$2500 \pm 100$	$0.52 \pm 0.09$	$0.01 \pm 0.005$	18/19

Table 2. Values of free parameters ( $T_1$ ,  $T_2$ ,  $\mathcal{E} \rightarrow V_1$ ,  $V_2$  and  $k$ ), normalization constant ( $N_0$ ),  $\chi^2$ , and degree of freedom (dof) corresponding to the curves in Fig. 2.

Collisions	Centrality	$T_1$ (GeV)	$T_2$ (GeV)	$V_1(fm^3)$	$V_2(fm^3)$	$k$	$N_0$	$\chi^2/\text{dof}$
Fig. 2 Au-Au 7.7 GeV	0-5%	$0.450 \pm 0.006$	$0.895 \pm 0.008$	$3000 \pm 200$	$1730 \pm 130$	$0.84 \pm 0.10$	$4 \pm 0.5$	7/26
	5-10%	$0.450 \pm 0.007$	$0.795 \pm 0.008$	$2900 \pm 160$	$1730 \pm 125$	$0.84 \pm 0.10$	$3.7 \pm 0.3$	11/26
	10-20%	$0.450 \pm 0.009$	$0.765 \pm 0.008$	$2643 \pm 190$	$1706 \pm 108$	$0.90 \pm 0.08$	$2.75 \pm 0.3$	6/26
	20-30%	$0.440 \pm 0.006$	$0.705 \pm 0.007$	$2543 \pm 160$	$1643 \pm 128$	$0.90 \pm 0.10$	$1.9 \pm 0.2$	2.5/26
	30-40%	$0.424 \pm 0.008$	$0.605 \pm 0.007$	$2400 \pm 170$	$1578 \pm 120$	$0.90 \pm 0.07$	$1.4 \pm 0.2$	0.4/26
	40-50%	$0.410 \pm 0.007$	$0.470 \pm 0.007$	$2300 \pm 170$	$1551 \pm 110$	$0.86 \pm 0.05$	$0.8 \pm 0.05$	9/25
	50-60%	$0.380 \pm 0.008$	$0.280 \pm 0.006$	$2240 \pm 160$	$1430 \pm 100$	$0.90 \pm 0.06$	$0.5 \pm 0.04$	0.2/24
	60-70%	$0.360 \pm 0.008$	$0.320 \pm 0.006$	$2000 \pm 169$	$1300 \pm 100$	$0.90 \pm 0.05$	$0.3 \pm 0.04$	2.5/25
Fig. 2 Au-Au 11.5 GeV	70-80%	$0.320 \pm 0.008$	$0.150 \pm 0.005$	$2000 \pm 170$	$1200 \pm 80$	$0.90 \pm 0.06$	$0.14 \pm 0.03$	8/24
	0-5%	$0.530 \pm 0.008$	$0.200 \pm 0.008$	$3300 \pm 201$	$1780 \pm 110$	$0.999 \pm 0.10$	$2.8 \pm 0.4$	14/25
	5-10%	$0.515 \pm 0.007$	$0.200 \pm 0.007$	$3200 \pm 197$	$1780 \pm 100$	$0.995 \pm 0.11$	$2.2 \pm 0.4$	1.6/26
	10-20%	$0.500 \pm 0.008$	$0.190 \pm 0.007$	$3100 \pm 170$	$1720 \pm 100$	$0.995 \pm 0.11$	$1.8 \pm 0.4$	1/26
	20-30%	$0.490 \pm 0.008$	$0.210 \pm 0.008$	$3000 \pm 150$	$1683 \pm 80$	$0.995 \pm 0.10$	$1.2 \pm 0.3$	13/26
	30-40%	$0.455 \pm 0.007$	$0.224 \pm 0.007$	$3000 \pm 134$	$1500 \pm 80$	$0.97 \pm 0.13$	$0.8 \pm 0.04$	0.5/26
	40-50%	$0.435 \pm 0.009$	$0.224 \pm 0.007$	$2960 \pm 161$	$1400 \pm 96$	$0.97 \pm 0.11$	$0.5 \pm 0.04$	9/25
	50-60%	$0.410 \pm 0.009$	$0.224 \pm 0.005$	$2800 \pm 152$	$1400 \pm 93$	$0.97 \pm 0.11$	$0.3 \pm 0.03$	12/25
Fig. 2 Au-Au 14.5 GeV	60-70%	$0.380 \pm 0.007$	$0.200 \pm 0.006$	$2760 \pm 150$	$1300 \pm 85$	$0.97 \pm 0.1$	$0.15 \pm 0.03$	16/25
	70-80%	$0.360 \pm 0.006$	$0.180 \pm 0.007$	$2500 \pm 120$	$1300 \pm 99$	$0.97 \pm 0.05$	$0.08 \pm 0.003$	19/26
	0-5%	$0.540 \pm 0.008$	$0.230 \pm 0.007$	$3500 \pm 170$	$1800 \pm 120$	$0.99 \pm 0.10$	$2.3 \pm 0.3$	14/22
	5-10%	$0.530 \pm 0.007$	$0.217 \pm 0.006$	$3300 \pm 190$	$1834 \pm 132$	$0.99 \pm 0.15$	$2.1 \pm 0.2$	1/22
	10-20%	$0.520 \pm 0.008$	$0.210 \pm 0.006$	$3200 \pm 150$	$1758 \pm 140$	$0.99 \pm 0.12$	$1.5 \pm 0.2$	1.5/22
	20-30%	$0.510 \pm 0.008$	$0.200 \pm 0.007$	$3200 \pm 119$	$1658 \pm 135$	$0.99 \pm 0.09$	$1 \pm 0.06$	1.2/22
	30-40%	$0.490 \pm 0.007$	$0.180 \pm 0.007$	$3000 \pm 140$	$1650 \pm 119$	$0.98 \pm 0.11$	$0.7 \pm 0.02$	1/22
	40-50%	$0.480 \pm 0.007$	$0.160 \pm 0.007$	$2800 \pm 152$	$1668 \pm 108$	$0.985 \pm 0.08$	$0.4 \pm 0.03$	0.3/22
Fig. 2 Au-Au 19.6 GeV	50-60%	$0.460 \pm 0.008$	$0.150 \pm 0.008$	$2700 \pm 120$	$1568 \pm 100$	$0.99 \pm 0.08$	$0.2 \pm 0.03$	8/22
	60-70%	$0.404 \pm 0.009$	$0.150 \pm 0.007$	$2600 \pm 106$	$1500 \pm 99$	$0.99 \pm 0.10$	$0.12 \pm 0.02$	0.3/22
	70-80%	$0.304 \pm 0.007$	$0.150 \pm 0.009$	$2400 \pm 80$	$1500 \pm 76$	$0.99 \pm 0.12$	$0.065 \pm 0.004$	1/22
	0-5%	$0.540 \pm 0.008$	$0.230 \pm 0.007$	$3700 \pm 170$	$2000 \pm 120$	$0.99 \pm 0.10$	$2.1 \pm 0.3$	13/26
	5-10%	$0.530 \pm 0.007$	$0.217 \pm 0.006$	$3700 \pm 190$	$1834 \pm 132$	$0.99 \pm 0.15$	$1.9 \pm 0.22$	3/25
	10-20%	$0.520 \pm 0.008$	$0.210 \pm 0.006$	$3600 \pm 150$	$1758 \pm 140$	$0.99 \pm 0.12$	$1.45 \pm 0.21$	2/20
	20-30%	$0.510 \pm 0.008$	$0.200 \pm 0.007$	$3500 \pm 119$	$1658 \pm 135$	$0.99 \pm 0.09$	$0.92 \pm 0.04$	19/20
	30-40%	$0.490 \pm 0.007$	$0.180 \pm 0.007$	$3300 \pm 140$	$1650 \pm 119$	$0.98 \pm 0.11$	$0.65 \pm 0.024$	7/20
Fig. 2 Au-Au 27 GeV	40-50%	$0.480 \pm 0.007$	$0.160 \pm 0.007$	$3100 \pm 152$	$1668 \pm 108$	$0.985 \pm 0.08$	$0.4 \pm 0.03$	13/20
	50-60%	$0.460 \pm 0.008$	$0.150 \pm 0.008$	$3100 \pm 120$	$1568 \pm 100$	$0.99 \pm 0.08$	$0.23 \pm 0.025$	8/20
	60-70%	$0.404 \pm 0.009$	$0.150 \pm 0.007$	$3000 \pm 106$	$1500 \pm 99$	$0.99 \pm 0.10$	$0.13 \pm 0.015$	12/20
	70-80%	$0.304 \pm 0.007$	$0.150 \pm 0.009$	$2900 \pm 80$	$1400 \pm 76$	$0.99 \pm 0.12$	$0.68 \pm 0.04$	7/20
	0-5%	$0.540 \pm 0.008$	$0.230 \pm 0.007$	$3500 \pm 170$	$2800 \pm 120$	$0.99 \pm 0.10$	$2.1 \pm 0.3$	13/26
	5-10%	$0.530 \pm 0.007$	$0.217 \pm 0.006$	$3300 \pm 190$	$2800 \pm 132$	$0.99 \pm 0.15$	$1.9 \pm 0.22$	3/25
	10-20%	$0.520 \pm 0.008$	$0.210 \pm 0.006$	$3205 \pm 150$	$2758 \pm 140$	$0.99 \pm 0.12$	$1.45 \pm 0.21$	2/20
	20-30%	$0.510 \pm 0.008$	$0.200 \pm 0.007$	$3200 \pm 119$	$2600 \pm 135$	$0.99 \pm 0.09$	$0.92 \pm 0.04$	19/20
Fig. 2 Au-Au 39 GeV	30-40%	$0.490 \pm 0.007$	$0.180 \pm 0.007$	$3000 \pm 140$	$2500 \pm 119$	$0.98 \pm 0.11$	$0.65 \pm 0.024$	7/20
	40-50%	$0.480 \pm 0.007$	$0.160 \pm 0.007$	$3000 \pm 152$	$2300 \pm 108$	$0.985 \pm 0.08$	$0.4 \pm 0.03$	13/20
	50-60%	$0.460 \pm 0.008$	$0.150 \pm 0.008$	$3000 \pm 120$	$2200 \pm 100$	$0.99 \pm 0.08$	$0.23 \pm 0.025$	8/20
	60-70%	$0.404 \pm 0.009$	$0.150 \pm 0.007$	$2500 \pm 106$	$2500 \pm 99$	$0.99 \pm 0.10$	$0.13 \pm 0.015$	12/20
	70-80%	$0.304 \pm 0.007$	$0.150 \pm 0.009$	$2400 \pm 80$	$1500 \pm 76$	$0.99 \pm 0.12$	$0.68 \pm 0.04$	7/20
	0-5%	$0.429 \pm 0.007$	$0.469 \pm 0.006$	$4000 \pm 260$	$2900 \pm 100$	$0.61 \pm 0.11$	$1.5 \pm 0.2$	2/23
	5-10%	$0.434 \pm 0.005$	$0.420 \pm 0.005$	$3934 \pm 210$	$2900 \pm 110$	$0.62 \pm 0.10$	$0.65 \pm 0.05$	8/23
	10-20%	$0.429 \pm 0.006$	$0.420 \pm 0.008$	$4000 \pm 160$	$2672 \pm 110$	$0.61 \pm 0.09$	$0.25 \pm 0.04$	4/23
Fig. 2 Au-Au 200 GeV	20-30%	$0.420 \pm 0.006$	$0.420 \pm 0.008$	$3800 \pm 170$	$2700 \pm 123$	$0.60 \pm 0.08$	$0.12 \pm 0.03$	10/23
	30-40%	$0.410 \pm 0.006$	$0.410 \pm 0.006$	$3900 \pm 200$	$2450 \pm 121$	$0.62 \pm 0.07$	$0.07 \pm 0.004$	14/23
	40-50%	$0.370 \pm 0.009$	$0.400 \pm 0.006$	$4000 \pm 174$	$2000 \pm 150$	$0.62 \pm 0.08$	$0.03 \pm 0.003$	17/23
	50-60%	$0.370 \pm 0.008$	$0.370 \pm 0.006$	$3800 \pm 180$	$2000 \pm 100$	$0.62 \pm 0.06$	$0.011 \pm 0.003$	11/23
	60-70%	$0.360 \pm 0.006$	$0.350 \pm 0.006$	$3600 \pm 160$	$2000 \pm 107$	$0.62 \pm 0.10$	$0.005 \pm 0.0004$	29/23
	70-80%	$0.350 \pm 0.006$	$0.346 \pm 0.006$	$3600 \pm 199$	$1800 \pm 130$	$0.62 \pm 0.08$	$0.0024 \pm 0.0005$	26/23
	0-5%	$0.489 \pm 0.009$	$0.469 \pm 0.008$	$5300 \pm 240$	$2900 \pm 130$	$0.63 \pm 0.13$	$43 \pm 6$	6/13
	5-10%	$0.479 \pm 0.008$	$0.469 \pm 0.008$	$4800 \pm 200$	$3200 \pm 130$	$0.63 \pm 0.10$	$18 \pm 2$	15/13
Fig. 2 Au-Au 200 GeV	10-15%	$0.469 \pm 0.008$	$0.463 \pm 0.009$	$4900 \pm 190$	$3000 \pm 130$	$0.635 \pm 0.09$	$7 \pm 1$	13/13
	15-20%	$0.459 \pm 0.008$	$0.460 \pm 0.007$	$4900 \pm 180$	$2800 \pm 135$	$0.635 \pm 0.09$	$3.3 \pm 0.3$	2/13
	20-30%	$0.450 \pm 0.006$	$0.460 \pm 0.008$	$4900 \pm 200$	$2620 \pm 128$	$0.62 \pm 0.07$	$0.07 \pm 0.004$	14/23
	30-40%	$0.450 \pm 0.009$	$0.440 \pm 0.007$	$4400 \pm 174$	$2900 \pm 150$	$0.62 \pm 0.09$	$0.03 \pm 0.003$	17/23
	40-50%	$0.448 \pm 0.009$	$0.420 \pm 0.007$	$4200 \pm 180$	$2900 \pm 140$	$0.62 \pm 0.06$	$0.011 \pm 0.003$	11/23
	50-60%	$0.426 \pm 0.007$	$0.420 \pm 0.007$	$4400 \pm 160$	$2280 \pm 137$	$0.62 \pm 0.12$	$0.005 \pm 0.0004$	29/23
	60-70%	$0.426 \pm 0.008$	$0.430 \pm 0.008$	$4400 \pm 199$	$2230 \pm 138$	$0.62 \pm 0.08$	$0.0024 \pm 0.0005$	26/23
	70-80%	$0.360 \pm 0.006$	$0.420 \pm 0.009$	$4300 \pm 160$	$2100 \pm 126$	$0.62 \pm 0.13$	$0.005 \pm 0.0004$	29/23
	80-92%	$0.420 \pm 0.008$	$0.412 \pm 0.007$	$4000 \pm 199$	$2230 \pm 100$	$0.62 \pm 0.09$	$0.0024 \pm 0.0005$	26/23

Table 3. Values of free parameters ( $T_1$ ,  $T_2$ ,  $V_1$ ,  $V_2$  and  $k$ ), normalization constant ( $N_0$ ),  $\chi^2$ , and degree of freedom (dof) corresponding to the curves in Fig. 3.

Collisions	Centrality	$T_1$ (GeV)	$T_2$ (GeV)	$V_1(fm^3)$	$V_2(fm^3)$	$k$	$N_0$	$\chi^2/\text{dof}$
Fig. 3	0–10%	$0.579 \pm 0.007$	$0.295 \pm 0.008$	$2000 \pm 150$	$1500 \pm 80$	$0.99 \pm 0.14$	$0.027 \pm 0.004$	10/6
Au-Au	10–20%	$0.560 \pm 0.008$	$0.105 \pm 0.006$	$2400 \pm 110$	$900 \pm 100$	$0.99 \pm 0.10$	$0.008 \pm 0.0006$	16/6
7.7 GeV	20–40%	$0.530 \pm 0.009$	$0.535 \pm 0.008$	$1800 \pm 90$	$1280 \pm 100$	$0.65 \pm 0.22$	$0.0028 \pm 0.0005$	4/6
	40–60%	$0.480 \pm 0.006$	$0.240 \pm 0.009$	$1700 \pm 100$	$1200 \pm 80$	$0.99 \pm 0.11$	$4 \times 10^{-4} \pm 6 \times 10^{-5}$	1.5/5
	60–80%	$0.420 \pm 0.009$	$0.355 \pm 0.008$	$1600 \pm 160$	$1270 \pm 40$	$0.96 \pm 0.20$	$4 \times 10^{-5} \pm 5 \times 10^{-6}$	3/3
Au-Au	0–10%	$0.622 \pm 0.007$	$0.205 \pm 0.007$	$3200 \pm 170$	$1100 \pm 70$	$0.95 \pm 0.015$	$0.007 \pm 0.0004$	7/6
11.5 GeV	10–20%	$0.582 \pm 0.008$	$0.195 \pm 0.007$	$3100 \pm 125$	$1000 \pm 75$	$0.98 \pm 0.12$	$0.0024 \pm 0.0005$	6/6
	20–40%	$0.560 \pm 0.009$	$0.200 \pm 0.006$	$3000 \pm 110$	$1000 \pm 100$	$0.98 \pm 0.16$	$7 \times 10^{-4} \pm 6 \times 10^{-5}$	3/6
	40–60%	$0.517 \pm 0.008$	$0.205 \pm 0.009$	$2000 \pm 100$	$900 \pm 80$	$0.97 \pm 0.13$	$8.5 \times 10^{-5} \pm 3 \times 10^{-6}$	2/5
	60–80%	$0.440 \pm 0.009$	$0.205 \pm 0.006$	$2900 \pm 120$	$700 \pm 50$	$0.99 \pm 0.08$	$7 \times 10^{-6} \pm 4 \times 10^{-7}$	6/4
Au-Au	0–10%	$0.639 \pm 0.007$	$0.755 \pm 0.008$	$3300 \pm 160$	$1600 \pm 90$	$0.99 \pm 0.09$	$0.004 \pm 0.0005$	9/6
14.5 GeV	10–20%	$0.620 \pm 0.009$	$0.612 \pm 0.009$	$3200 \pm 110$	$1500 \pm 90$	$0.26 \pm 0.07$	$8 \times 10^{-4} \pm 4 \times 10^{-5}$	6/6
	20–40%	$0.588 \pm 0.006$	$0.605 \pm 0.008$	$3400 \pm 120$	$1120 \pm 100$	$0.98 \pm 0.21$	$3.5 \times 10^{-4} \pm 6 \times 10^{-5}$	10/6
	40–60%	$0.534 \pm 0.007$	$0.631 \pm 0.009$	$3000 \pm 90$	$1300 \pm 90$	$0.96 \pm 0.19$	$6 \times 10^{-5} \pm 5 \times 10^{-6}$	2/5
	60–80%	$0.487 \pm 0.009$	$0.455 \pm 0.008$	$3000 \pm 90$	$1000 \pm 70$	$0.5 \pm 0.10$	$3.3 \times 10^{-6} \pm 5 \times 10^{-7}$	22/4
Au-Au	0–10%	$0.640 \pm 0.006$	$0.600 \pm 0.008$	$3300 \pm 130$	$2200 \pm 90$	$0.99 \pm 0.21$	$0.0027 \pm 0.0004$	12/6
19.6 GeV	10–20%	$0.614 \pm 0.008$	$0.615 \pm 0.009$	$3500 \pm 100$	$1600 \pm 70$	$0.96 \pm 0.14$	$9 \times 10^{-4} \pm 4 \times 10^{-5}$	11/6
	20–40%	$0.588 \pm 0.007$	$0.605 \pm 0.008$	$3500 \pm 110$	$1600 \pm 80$	$0.97 \pm 0.17$	$2.0 \times 10^{-4} \pm 4 \times 10^{-5}$	5/6
	40–60%	$0.535 \pm 0.006$	$0.605 \pm 0.010$	$3000 \pm 100$	$1900 \pm 80$	$0.95 \pm 0.10$	$3.6 \times 10^{-5} \pm 5 \times 10^{-6}$	2/5
	60–80%	$0.468 \pm 0.007$	$0.405 \pm 0.009$	$2700 \pm 130$	$1830 \pm 70$	$0.99 \pm 0.15$	$3.8 \times 10^{-6} \pm 4 \times 10^{-7}$	13/4
Au-Au	0–10%	$0.641 \pm 0.007$	$0.634 \pm 0.010$	$3700 \pm 100$	$2308 \pm 160$	$0.88 \pm 0.16$	$0.00135 \pm 0.0004$	6/6
27 GeV	10–20%	$0.614 \pm 0.005$	$0.650 \pm 0.010$	$3600 \pm 110$	$2250 \pm 180$	$0.99 \pm 0.16$	$6 \times 10^{-4} \pm 5 \times 10^{-5}$	3/6
	20–40%	$0.582 \pm 0.006$	$0.605 \pm 0.009$	$3000 \pm 115$	$2715 \pm 180$	$0.99 \pm 0.18$	$2 \times 10^{-4} \pm 4 \times 10^{-5}$	4/6
	40–60%	$0.436 \pm 0.009$	$0.605 \pm 0.007$	$2900 \pm 130$	$2500 \pm 170$	$0.97 \pm 0.12$	$3 \times 10^{-5} \pm 4 \times 10^{-6}$	0.1/5
	60–80%	$0.594 \pm 0.008$	$0.453 \pm 0.008$	$3000 \pm 120$	$2236 \pm 190$	$0.09 \pm 0.11$	$7 \times 10^{-7} \pm 3 \times 10^{-8}$	7/5
Au-Au	0–10%	$0.654 \pm 0.007$	$0.305 \pm 0.009$	$3500 \pm 106$	$2908 \pm 194$	$0.96 \pm 0.16$	$0.0011 \pm 0.0004$	9/6
39 GeV	10–20%	$0.618 \pm 0.008$	$0.305 \pm 0.007$	$3600 \pm 103$	$2640 \pm 152$	$0.99 \pm 0.13$	$4.2 \times 10^{-4} \pm 4 \times 10^{-5}$	4/6
	20–40%	$0.588 \pm 0.009$	$0.245 \pm 0.007$	$3300 \pm 105$	$2800 \pm 175$	$0.98 \pm 0.14$	$1.2 \times 10^{-4} \pm 3 \times 10^{-5}$	6/6
	40–60%	$0.540 \pm 0.010$	$0.371 \pm 0.007$	$3600 \pm 105$	$2300 \pm 160$	$0.99 \pm 0.15$	$2 \times 10^{-5} \pm 6 \times 10^{-6}$	0.6/6
	60–80%	$0.465 \pm 0.008$	$0.527 \pm 0.007$	$3500 \pm 100$	$2200 \pm 175$	$0.99 \pm 0.13$	$1.6 \times 10^{-6} \pm 4 \times 10^{-7}$	13/5
Au-Au	0–10%	$0.690 \pm 0.007$	$0.505 \pm 0.008$	$3800 \pm 120$	$3200 \pm 190$	$0.99 \pm 0.14$	$8.5 \times 10^{-4} \pm 4 \times 10^{-5}$	5/6
62.4 GeV	10–20%	$0.663 \pm 0.008$	$0.604 \pm 0.010$	$4000 \pm 240$	$2830 \pm 180$	$0.96 \pm 0.13$	$2.6 \times 10^{-4} \pm 5 \times 10^{-5}$	4/6
	20–40%	$0.630 \pm 0.009$	$0.463 \pm 0.008$	$3700 \pm 100$	$2900 \pm 90$	$0.98 \pm 0.10$	$8 \times 10^{-5} \pm 4 \times 10^{-6}$	6/6
	40–60%	$0.590 \pm 0.007$	$0.532 \pm 0.009$	$3400 \pm 115$	$3000 \pm 85$	$0.97 \pm 0.20$	$1.4 \times 10^{-5} \pm 4 \times 10^{-6}$	22/6
	60–80%	$0.515 \pm 0.007$	$0.297 \pm 0.010$	$4000 \pm 110$	$2130 \pm 70$	$0.96 \pm 0.17$	$1.1 \times 10^{-6} \pm 5 \times 10^{-7}$	6/5
Au-Au	0–10%	$0.800 \pm 0.008$	$0.434 \pm 0.009$	$4300 \pm 100$	$3300 \pm 200$	$0.96 \pm 0.21$	$5.8 \times 10^{-4} \pm 4 \times 10^{-5}$	12/6
200 GeV	10–20%	$0.745 \pm 0.007$	$0.932 \pm 0.008$	$4000 \pm 110$	$3400 \pm 210$	$0.97 \pm 0.12$	$2.3 \times 10^{-4} \pm 5 \times 10^{-5}$	5/6
	20–40%	$0.700 \pm 0.008$	$0.576 \pm 0.009$	$4800 \pm 120$	$2430 \pm 180$	$0.95 \pm 0.17$	$6.8 \times 10^{-5} \pm 5 \times 10^{-6}$	15/6
	40–40%	$0.650 \pm 0.009$	$0.679 \pm 0.008$	$4100 \pm 100$	$2900 \pm 190$	$0.93 \pm 0.15$	$1.25 \times 10^{-5} \pm 4 \times 10^{-6}$	1/6
	60–80%	$0.550 \pm 0.010$	$0.705 \pm 0.007$	$4000 \pm 100$	$2800 \pm 80$	$0.96 \pm 0.13$	$1.4 \times 10^{-6} \pm 3 \times 10^{-7}$	2/5



trality decreases, the number of participants decreases, which leads the system to equilibrium state in a steady manner. We also observed that the kinetic freeze-out volume is mass dependent. The lighter the particle, the larger the kinetic freeze-out volume. This observation shows the early freeze-out of the heavier particles compared to the lighter ones, and this may indicate different freeze-out surfaces for various particles. One can found such results in literature [56, 57].

Figure 7 and 8 are also similar to figure 5 and 6, but they show the energy and centrality dependent mean transverse momentum ( $\langle p_T \rangle$ ) and initial temperature ( $T_i$ ) respectively. We have analyzed the mean  $p_T$  ( $\langle p_T \rangle$ ) and the root-mean-square  $p_T$  ( $\sqrt{\langle p_T^2 \rangle}$ ) over  $\sqrt{2}$  ( $\sqrt{\langle p_T^2 \rangle}/\sqrt{2}$ ) which are calculated from the fit function over a given  $p_T$  range and it is noteworthy that  $p_T$  used to obtain the initial temperature and mean  $p_T$  is extrapolated up to zero. According to string percolation model [58–60], ( $\sqrt{\langle p_T^2 \rangle}/\sqrt{2}$ ) represent the initial temperature ( $T_i$ ). One can see that that  $\langle p_T \rangle$  and  $T_i$  increases with energy from 7.7 to 14.5 and then remains unchanged up to 39 GeV and then again rises at 62.4 and 200 GeV. Like  $T$  and  $V$ , both  $\langle p_T \rangle$  and  $T_i$  increases from peripheral to central collisions. Both  $\langle p_T \rangle$  and  $T_i$  are mass dependent. Heavier the particle, larger the  $\langle p_T \rangle$  and  $T_i$ .

Although the parameters  $T$ ,  $V$ ,  $T_i$  and  $T_0$  are extracted from the model, in fact they are based on the fit to experimental data. In ref. [61, 62]  $T_i$  does not depend on the model, but is equal to  $\sqrt{\langle p_T^2 \rangle}/\sqrt{2}$  and can be obtained from the  $p_T$  spectra, and we can also obtain it from the data directly.

Figure 9 shows the relation between the effective temperature and rest mass of the particle. Deuteron and triton at different energies are put together in different panels and are fitted by the linear equation by the relation  $T = T_0 + am_0$ , where  $T_0$  is the intercept and  $m_0$  is the slope. The intercepts of the emission source is  $T_0$  for massless particles e.g the intercepts starts from  $m_0=0$ . Therefore, it does not matter whether two or three data points. The intercepts from two, three and five data points may be different, that indicates the multiple temperature, or different stages or different times of formation of different particles. The intercepts and slopes with the value of  $\chi^2$  obtained by the linear function are listed in table 3. The effective temperature versus rest mass of the particle at 7.7, 11.5, 14.5, 19.6, 27, 39, 62.4 and 200 GeV are presented in panels (a), (b), (c), (d), (e), (f), (g) and (h) respectively in 0–10%, 10–20% and 20–40% centrality bins. The last centrality classes are

missing because they are different for deuteron and triton (40–60% and 60–80% for deuteron, and 40–80% for triton). In order to include them in the present work, we have to distribute 40–80% centrality bin of triton, and it is not an easy job, so we skip it and showed the first three centrality classes. It should be noted that we also skipped to include  $K^+$  and  $p$  in the above relation because of their different centrality intervals from  $d$  and  $t$ . In fact we only presented a few centrality classes of  $d$  and  $t$  which were the same, in order to show that how to extract  $T_0$  by the alternative method. In fig. 7, the intercepts between the effective temperatures and the rest mass of the particles are regarded as the average kinetic freeze-out temperature [9, 16].

Figure 10 shows the dependence of kinetic freeze-out temperature. The symbols from up to downward and from left to right shows the dependence of kinetic freeze-out temperature on centrality and energy respectively. We noticed three trends of  $T_0$  with rising the collision energy, (1) from 7.7 to 14.5 GeV which is increasing, (2) 14.5 to 39 GeV which remains consistent, and (3) again increasing trend, which indicate towards different interaction mechanisms in  $\sqrt{s_{NN}}=14.5-39$  GeV,  $\sqrt{s_{NN}} < 14.5$  GeV and  $\sqrt{s_{NN}} > 39$  GeV. We believe that if, the baryon-dominated effect plays more important role at below 14.5 GeV in AA collisions, the meson-dominated effect should play more important role at above 14.5 GeV. In case of baryon-domination, the system deposits less energy, and then the system has low excitation degree and temperature, However the case is opposite in meson dominated case. In fact, 14.5 GeV is a particular energy that may need more attention to be paid. It seems that the phase transition occurs in part volume from 14.5 GeV to 39 GeV, where 14.5 GeV may be the onset energy of the part phase transition and 39 GeV is the whole phase transition. The range of critical energy is 14.5 GeV to 39 GeV. If the region from 14.5 to 39 GeV in the excitation functions of  $T_0$  is regarded as a reflection of the formation of QGP liquid drop, the quick rise of  $T_0$  at 62.4 and 200 GeV is a reflection of higher temperature QGP liquid drop due to larger energy deposition. At 62.4 and 200 GeV, the higher collision energy should result in creation of larger energy density and blast wave, and then higher  $T_0$ . It should be noted that, the above discussion on the excitation function of  $T_0$  presented in Fig. 10 is also suitable to the excitation function of  $T$  presented in Fig. 5 and  $T_i$  in fig. 8, though the effect of flow is included in the former. We believe that  $T_i$ ,  $T$  and  $T_0$  has the same trend because the later two are the reflection of the former.

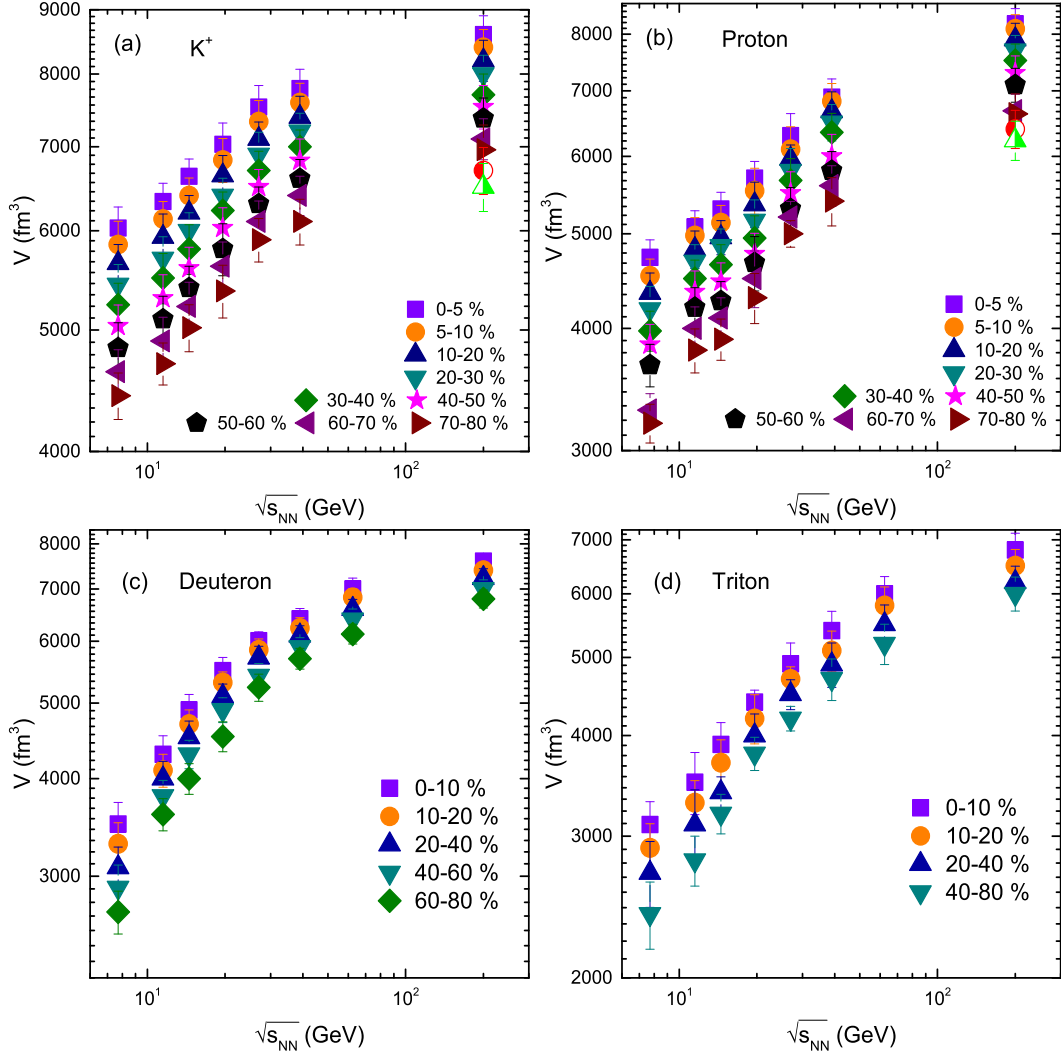


Fig. 6. Similar to fig. 5, but it presents the dependence of kinetic freeze-out volume on energy and centrality for  $K^+$ ,  $p$ ,  $d$  and  $t$ .

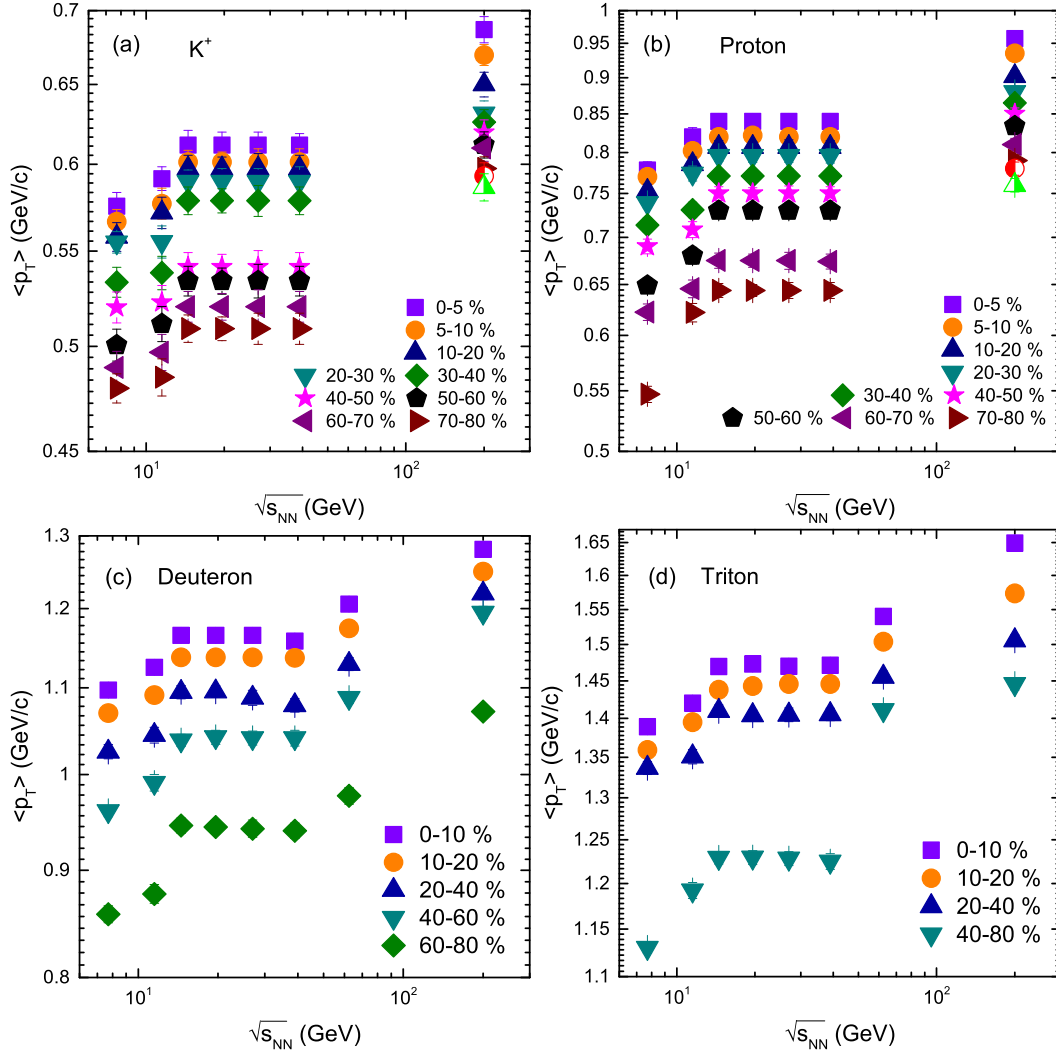


Fig. 7. Similar to fig. 5, but it presents the dependence of mean transverse momentum on energy and centrality for  $K^+$ ,  $p$ ,  $d$  and  $t$ .

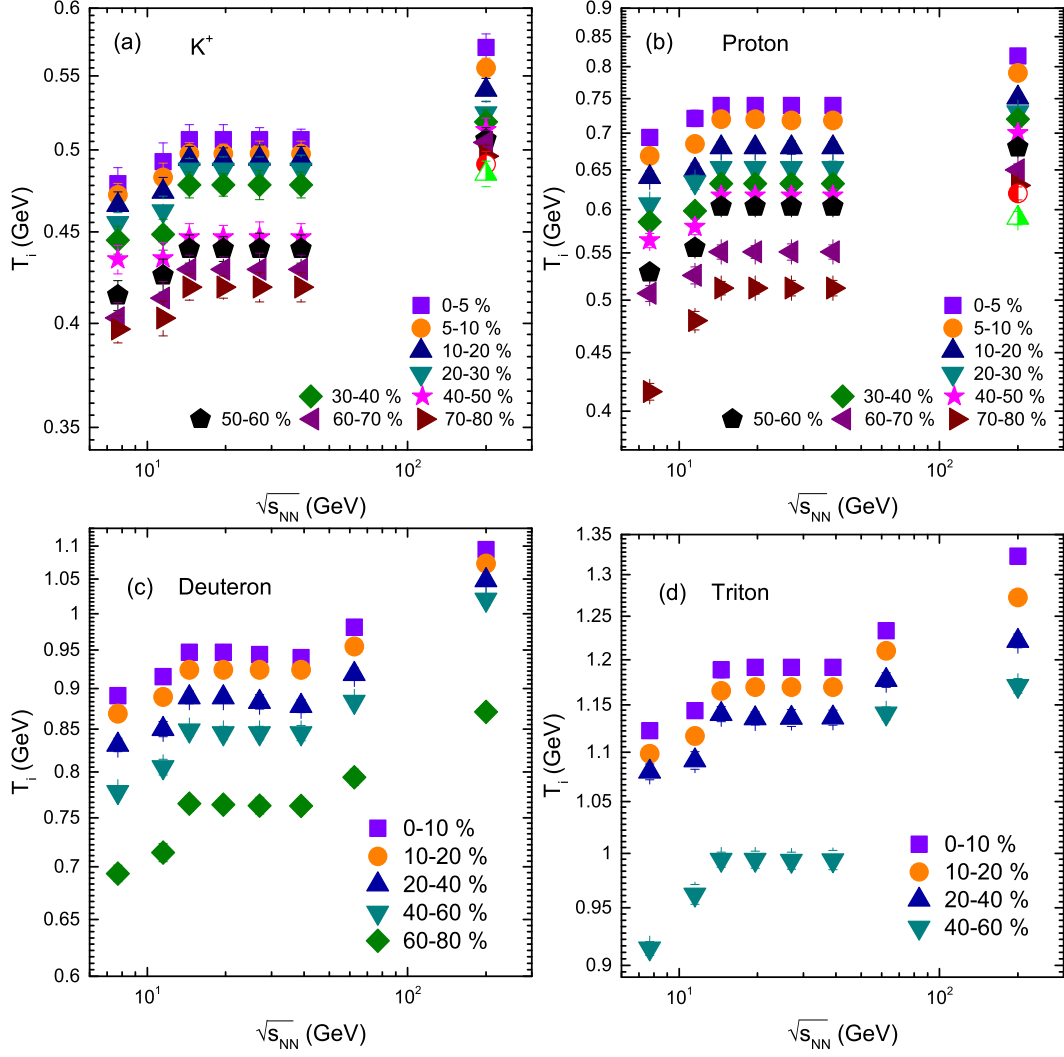


Fig. 8. Similar to fig. 5, but it presents the dependence of initial temperature on energy and centrality for  $K^+$ ,  $p$ ,  $d$  and  $t$ .

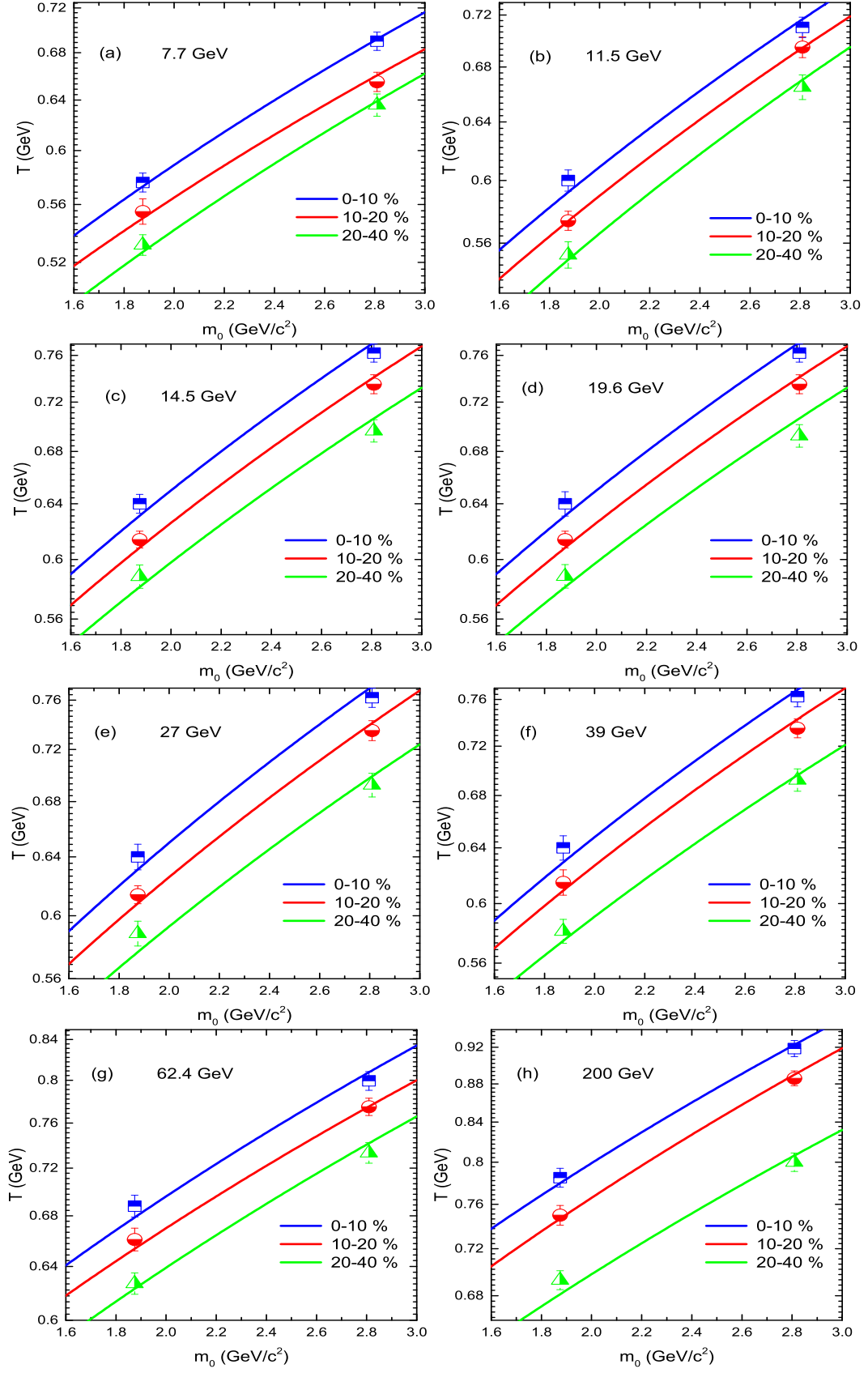


Fig. 9. Relation between the effective temperature and  $m_0$ .

Table 4. Values of free parameters ( $T_1$ ,  $T_2$ ,  $\mathcal{E} \rightarrow V_1$ ,  $V_2$  and  $k$ ), normalization constant ( $N_0$ ),  $\chi^2$ , and degree of freedom (dof) corresponding to the curves in Fig. 4.

Collisions	Centrality	$T_1$ (GeV)	$T_2$ (GeV)	$V_1(fm^3)$	$V_2(fm^3)$	$k$	$N_0$	$\chi^2/\text{dof}$
Fig. 4	0-10%	$0.691 \pm 0.005$	$0.595 \pm 0.006$	$2000 \pm 130$	$1100 \pm 80$	$0.99 \pm 0.24$	$1.2 \times 10^{-4} \pm 3 \times 10^{-5}$	7/2
Au-Au	10-20%	$0.657 \pm 0.006$	$0.595 \pm 0.005$	$1800 \pm 108$	$1100 \pm 100$	$0.97 \pm 0.20$	$3.9 \times 10^{-5} \pm 4 \times 10^{-6}$	4/2
7.7 GeV	20-40%	$0.640 \pm 0.007$	$0.585 \pm 0.006$	$1600 \pm 143$	$1100 \pm 110$	$0.94 \pm 0.22$	$9.7 \times 10^{-6} \pm 5 \times 10^{-7}$	5/2
	40-60%	$0.650 \pm 0.006$	$0.450 \pm 0.008$	$1300 \pm 120$	$1100 \pm 110$	$0.11 \pm 0.02$	$2.4 \times 10^{-6} \pm 4 \times 10^{-7}$	2/0
Au-Au	0-10%	$0.200 \pm 0.006$	$0.830 \pm 0.006$	$3000 \pm 150$	$1500 \pm 160$	$0.19 \pm 0.01$	$3.9 \times 10^{-5} \pm 4 \times 10^{-6}$	2/2
11.5 GeV	10-20%	$0.200 \pm 0.005$	$0.710 \pm 0.006$	$2000 \pm 100$	$1300 \pm 115$	$0.03 \pm 0.006$	$1.5 \times 10^{-5} \pm 3 \times 10^{-6}$	4/2
	20-40%	$0.650 \pm 0.007$	$0.664 \pm 0.007$	$1800 \pm 120$	$1300 \pm 105$	$0.98 \pm 0.26$	$1.9 \times 10^{-6} \pm 6 \times 10^{-7}$	6/-
	40-80%	$0.540 \pm 0.005$	$0.470 \pm 0.007$	$1700 \pm 90$	$1100 \pm 110$	$0.80 \pm 0.23$	$4.2 \times 10^{-7} \pm 6 \times 10^{-8}$	1/1
Au-Au	0-10%	$0.767 \pm 0.006$	$0.295 \pm 0.007$	$2200 \pm 140$	$1700 \pm 110$	$0.99 \pm 0.25$	$0.0013 \pm 0.0004$	6/2
14.5 GeV	10-20%	$0.739 \pm 0.004$	$0.295 \pm 0.009$	$2400 \pm 150$	$1300 \pm 100$	$0.99 \pm 0.30$	$3.6 \times 10^{-6} \pm 5 \times 10^{-7}$	4/2
	20-40%	$0.700 \pm 0.006$	$0.340 \pm 0.006$	$2000 \pm 135$	$1400 \pm 120$	$0.99 \pm 0.27$	$9.6 \times 10^{-7} \pm 3 \times 10^{-8}$	32/2
	40-80%	$0.460 \pm 0.006$	$0.525 \pm 0.006$	$2000 \pm 90$	$1200 \pm 90$	$0.38 \pm 0.19$	$2.7 \times 10^{-7} \pm 5 \times 10^{-8}$	10/2
Au-Au	0-10%	$0.767 \pm 0.006$	$0.295 \pm 0.007$	$3200 \pm 135$	$1200 \pm 120$	$0.99 \pm 0.25$	$4.7 \times 10^{-6} \pm 6 \times 10^{-7}$	3/2
19.6 GeV	10-20%	$0.740 \pm 0.004$	$0.295 \pm 0.009$	$3000 \pm 170$	$1200 \pm 126$	$0.99 \pm 0.30$	$1.5 \times 10^{-6} \pm 5 \times 10^{-7}$	5/2
	20-40%	$0.696 \pm 0.006$	$0.340 \pm 0.006$	$3000 \pm 140$	$1000 \pm 114$	$0.99 \pm 0.27$	$3.3 \times 10^{-7} \pm 7 \times 10^{-8}$	6/2
	40-80%	$0.650 \pm 0.007$	$0.425 \pm 0.009$	$2000 \pm 90$	$1800 \pm 90$	$0.58 \pm 0.19$	$4.2 \times 10^{-8} \pm 6 \times 10^{-9}$	1/2
Au-Au	0-10%	$0.910 \pm 0.005$	$0.205 \pm 0.006$	$3000 \pm 150$	$1910 \pm 150$	$0.79 \pm 0.20$	$2.7 \times 10^{-6} \pm 4 \times 10^{-7}$	4/2
27 GeV	10-20%	$0.740 \pm 0.006$	$0.293 \pm 0.007$	$2600 \pm 135$	$2100 \pm 133$	$0.99 \pm 0.18$	$8.6 \times 10^{-7} \pm 5 \times 10^{-8}$	4/2
	20-40%	$0.696 \pm 0.006$	$0.340 \pm 0.006$	$3400 \pm 150$	$1100 \pm 142$	$0.99 \pm 0.22$	$2.2 \times 10^{-7} \pm 6 \times 10^{-8}$	3/2
	40-80%	$0.579 \pm 0.005$	$0.425 \pm 0.007$	$3200 \pm 120$	$1000 \pm 128$	$0.85 \pm 0.19$	$4 \times 10^{-8} \pm 5 \times 10^{-9}$	0.6/1
Au-Au	0-10%	$0.928 \pm 0.007$	$0.291 \pm 0.008$	$3000 \pm 154$	$2400 \pm 160$	$0.74 \pm 0.22$	$1.5 \times 10^{-6} \pm 4 \times 10^{-7}$	12/2
39 GeV	10-20%	$0.740 \pm 0.007$	$0.293 \pm 0.008$	$3000 \pm 150$	$2100 \pm 142$	$0.99 \pm 0.18$	$4.7 \times 10^{-7} \pm 5 \times 10^{-8}$	5/2
	20-40%	$0.696 \pm 0.006$	$0.325 \pm 0.006$	$3200 \pm 160$	$1700 \pm 150$	$0.99 \pm 0.20$	$1.2 \times 10^{-7} \pm 4 \times 10^{-8}$	4/2
	40-80%	$0.715 \pm 0.005$	$0.410 \pm 0.007$	$2500 \pm 150$	$2200 \pm 130$	$0.45 \pm 0.10$	$3.3 \times 10^{-8} \pm 7 \times 10^{-9}$	2/2
Au-Au	0-10%	$0.260 \pm 0.006$	$0.880 \pm 0.006$	$3200 \pm 140$	$2800 \pm 160$	$0.13 \pm 0.04$	$8 \times 10^{-7} \pm 6 \times 10^{-8}$	8/0
62.4 GeV	10-20%	$0.780 \pm 0.005$	$0.267 \pm 0.008$	$3000 \pm 160$	$2800 \pm 157$	$0.99 \pm 0.23$	$2.6 \times 10^{-7} \pm 6 \times 10^{-8}$	6/0
	20-40%	$0.740 \pm 0.007$	$0.405 \pm 0.006$	$3000 \pm 140$	$2500 \pm 170$	$0.98 \pm 0.20$	$8.2 \times 10^{-8} \pm 5 \times 10^{-9}$	13/0
	40-80%	$0.700 \pm 0.008$	$0.400 \pm 0.006$	$3200 \pm 150$	$2000 \pm 150$	$0.99 \pm 0.28$	$1.6 \times 10^{-8} \pm 4 \times 10^{-9}$	5/0
Au-Au	0-10%	$0.925 \pm 0.009$	$0.289 \pm 0.009$	$4000 \pm 160$	$2800 \pm 170$	$0.99 \pm 0.24$	$2.4 \times 10^{-7} \pm 6 \times 10^{-8}$	1/-
200 GeV	10-20%	$0.892 \pm 0.008$	$0.276 \pm 0.006$	$4000 \pm 170$	$2500 \pm 140$	$0.99 \pm 0.17$	$1.1 \times 10^{-7} \pm 5 \times 10^{-8}$	3/-
	20-40%	$0.812 \pm 0.007$	$0.250 \pm 0.007$	$4000 \pm 150$	$2200 \pm 140$	$0.98 \pm 0.23$	$3.6 \times 10^{-8} \pm 5 \times 10^{-9}$	4/-
	40-80%	$0.700 \pm 0.007$	$0.995 \pm 0.007$	$4000 \pm 150$	$2000 \pm 140$	$0.90 \pm 0.23$	$8 \times 10^{-9} \pm 4 \times 10^{-10}$	9/-

We would like to specify that we included  $K^+$  and  $p$  with  $d$  and  $t$  in order to check the difference in trend of the parameters of  $K^+$  and  $p$  from  $d$  and  $t$ . There is no difference observed in the trend of parameters for these particles. Different particle species can give information about the differences in their emission but they are not responsible to cause any difference in the trend of the parameters. In deed, different models and methods used in the extraction of the parameters can give their different trend. Such studies are present in literature [37, 52, 63, 64, 65]. Furthermore, it can also be seen that the temperature of  $t$  is the largest and that for  $K^+$  is the lowest which shows that heavier particles decouple early from the system. The effective temperature, initial temperature and kinetic freeze-out temperature has the same behavior with increasing energy, and hence their explanation is the same. Furthermore, like the effective and initial temperature, the kinetic freeze-out temperature also increases with centrality which indicates that the central collision is more harsh and the energy deposited in central collisions system is larger compared to the peripheral collisions, and hence it results in larger temperature. The larger  $T$  ( $T$  or  $T_0$ ) in central collisions

means that the particles in central collisions decouple from the system more early compared to the peripheral collisions.

In addition, we observed that the initial temperature is larger than the effective temperature, and the later is larger than the kinetic freeze-out temperature. In general, the chemical freeze-out temperature occurs between the initial and kinetic freeze-out temperatures, and is roughly equal to the effective temperature. This sequence is consistent with the order of time evolution of the interacting system, although both the effective and kinetic freeze-out temperatures are extracted at the kinetic/thermal freeze-out. However, the four temperatures can not be compared directly in most cases due to different thermometric scales being used. For example, one use thermometric scales in thermal and statistical physics, a method is needed to unify different thermometric scales in subatomic physics, but it is beyond the focus of the present work to structure the method. This issue shall not be discussed further in the present work. It is noteworthy that the values of temperatures in the present work are higher than the normal values because different scale is used in their extraction.

Table 5. Values of slopes and intercepts in different types of collisions at the RHIC.

Collisions	$\sqrt{s_{NN}}$ ( $\sqrt{s}$ )	centrality	<i>slope</i>	<i>intercept</i>	$\chi^2$
Au-Au	7.7 GeV	0–10%	$0.127 \pm 0.007$	$0.335 \pm 0.007$	0.2
		10–20%	$0.118 \pm 0.008$	$0.323 \pm 0.006$	0.7
		20–40%	$0.120 \pm 0.008$	$0.302 \pm 0.008$	0.4
Au-Au	11.5 GeV	0–10%	$0.133 \pm 0.008$	$0.343 \pm 0.008$	1.7
		10–20%	$0.129 \pm 0.006$	$0.332 \pm 0.009$	0.006
		20–40%	$0.126 \pm 0.008$	$0.308 \pm 0.006$	0.5
Au-Au	14.5 GeV	0–10%	$0.150 \pm 0.007$	$0.350 \pm 0.007$	2
		10–20%	$0.142 \pm 0.007$	$0.342 \pm 0.007$	0.9
		20–40%	$0.134 \pm 0.007$	$0.330 \pm 0.008$	2
Au-Au	19.6 GeV	0–10%	$0.150 \pm 0.006$	$0.350 \pm 0.008$	2
		10–20%	$0.142 \pm 0.007$	$0.342 \pm 0.005$	0.9
		20–40%	$0.134 \pm 0.007$	$0.330 \pm 0.008$	3
Au-Au	27 GeV	0–10%	$0.150 \pm 0.007$	$0.350 \pm 0.006$	2
		10–20%	$0.142 \pm 0.006$	$0.342 \pm 0.006$	0.9
		20–40%	$0.134 \pm 0.007$	$0.331 \pm 0.007$	0.8
Au-Au	39 GeV	0–10%	$0.150 \pm 0.008$	$0.350 \pm 0.007$	2
		10–20%	$0.143 \pm 0.006$	$0.341 \pm 0.006$	0.1
		20–40%	$0.130 \pm 0.007$	$0.331 \pm 0.007$	0.8
Au-Au	62.4 GeV	0–10%	$0.138 \pm 0.009$	$0.420 \pm 0.006$	2
		10–20%	$0.130 \pm 0.008$	$0.410 \pm 0.007$	0.8
		20–40%	$0.127 \pm 0.008$	$0.385 \pm 0.009$	1
Au-Au	200 GeV	0–10%	$0.153 \pm 0.007$	$0.493 \pm 0.006$	0.6
		10–20%	$0.153 \pm 0.008$	$0.460 \pm 0.008$	0.3
		20–40%	$0.134 \pm 0.007$	$0.430 \pm 0.008$	0.7

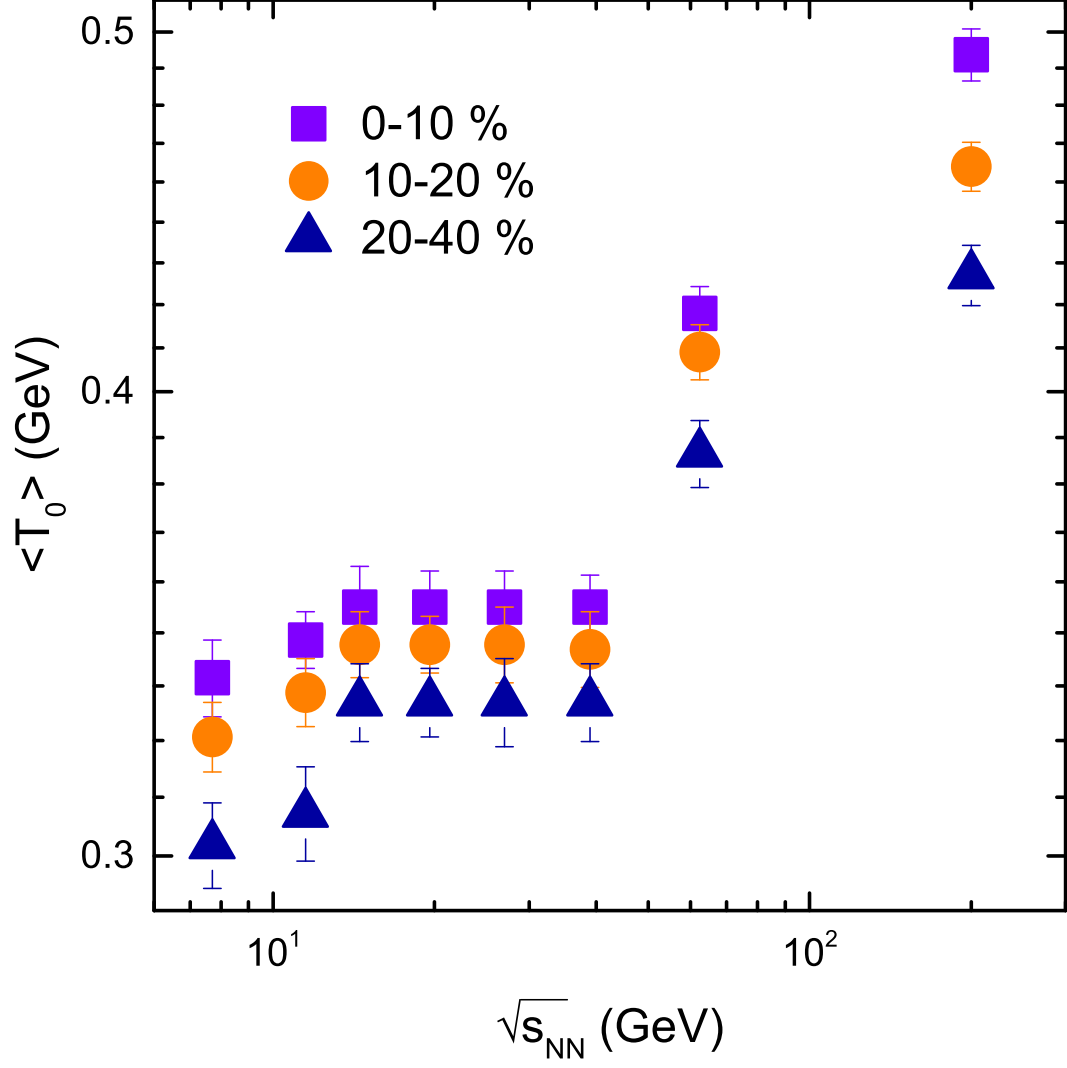


Fig. 10. Dependence of average kinetic freeze-out temperature on energy and centrality.



Before going to conclusion, we would like to point out that we obtained the initial temperature from root-mean-square  $p_T$  taking analogy from string percolation model which is valid in the present work because Hagedorn thermal model is a hybrid model. We use the Monte-carlo simulation in the extraction of  $T_i$ . There are many different methods by which we can extract  $T_i$ , such as we can get  $\langle p_T \rangle$  and  $\sqrt{\langle p_T^2 \rangle}$  from the combination of data points also and fit function in the present work. Indeed, the  $p_T$  spectrum can be divided into two or three regions according to the measured and un-measured  $p_T$  ranges. One can use the data points in the measured  $p_T$  range and use the fit function only to estimate to the un-measured  $p_T$  range in order to obtain  $\langle p_T \rangle$  and  $\sqrt{\langle p_T^2 \rangle}$ . The projectile and target participant sources contribute equally to  $\langle p_T \rangle$  in each nucleon-nucleon collision in AA collisions. According to the framework of multi-source thermal model, [18, 66, 67] each projectile and target source contribute a fraction of 1/2 to  $\langle p_T \rangle$ , i.e  $\langle p_T \rangle / 2$ , which contributes the thermal motion and flow effect together. Let us consider  $k_0(1 - k_0)$  represents the contribution fraction of thermal motion (flow effect), one can define empirically

$$T_0 \equiv \frac{k_0 \langle p_T \rangle}{2}, \quad (10)$$

and

$$\beta_T \equiv \frac{(1 - k_0) \langle p_T \rangle}{2m_0\bar{\gamma}}, \quad (11)$$

where  $\bar{\gamma}$  represents the lorentz factor of the considered particle and

$$k_0 = 0.30 - 0.01 \ln(\sqrt{s_{NN}}), \quad (12)$$

is a parameterized representation. The effective temperature in a recent work [68] is proportional to  $\langle p_T \rangle$  and the kinetic freeze-out temperature is proportional to the effective temperature, although the effective temperature in [68] and in our present work is not the same. This method is diverting the focus of the present work, so will not discuss it further.

In short, if we consider  $O - xyz$  coordinate system, the momentum components in this system are

$$p_x = p_T \cos\theta, \quad (13)$$

$$p_y = p_T \sin\theta, \quad (14)$$

and

$$p_z = p_T \cot\theta = p \cos\theta, \quad (15)$$

so, we have the relation between three components  $p_x$ ,  $p_y$  and  $p_z$  of the momentum  $p$  to be

$$\sqrt{\langle p_x^2 \rangle} = \sqrt{\langle p_y^2 \rangle} = \sqrt{\langle p_z^2 \rangle} = \sqrt{\langle p_T^2 \rangle} / 2, \quad (16)$$

where  $\sqrt{\langle p_x^2 \rangle}$ ,  $\sqrt{\langle p_y^2 \rangle}$  and  $\sqrt{\langle p_z^2 \rangle}$  are root-mean square components and  $T_i$  can be given by anyone of these components. It should be noted that above isotropic assumption is only performed in the source rest frame. However there are interactions among various sources, and  $p_z$  is lorentz boosted from one source to another one. This renders that there are anisotropic momentum components in the final state.

## 4 Conclusions

The main observations and conclusions are summarized here.

(a) The transverse momentum spectra of the kaon, proton, deuteron and triton produced in various centrality intervals in Au-Au collisions at RHIC energies have been analyzed by Hagedorn thermal model. The model results are in good agreement with the experimental data in the special  $p_T$  range measured by STAR Collaboration.

(b) Effective temperature  $T$ , initial temperature  $T_i$ , kinetic freeze-out temperature ( $T_0$ ), and the mean transverse momentum ( $\langle p_T \rangle$ ) increases from 7.7 GeV to 14.5 GeV and then keeps consistent up to 39 GeV, and once again grows at 62.4 and 200 GeV, while the kinetic freeze-out volume ( $V$ ) has an increasing trend with increasing energy due to longer evolution time for partonic system at higher energies.

(c) Due to low energy deposition, the system from 7.7 GeV to 14.5 GeV is baryon influenced and there is no phase transition. The phase transition in the system starts from 14.5 GeV in part volume and encounter from baryon-influenced to meson-influenced due to the phase transition in larger and larger volume in 14.5 GeV to 39 GeV. The identified boundaries exists for the three energy ranges which exhibit three different mechanisms of interaction and evolution process.

(d) The initial temperature and effective temperature for triton are larger than deuteron, and the later is larger than proton and kaon. Kaon has the lowest values for the temperatures while the case for kinetic freeze-out volume is opposite where the heaviest particle has the lowest  $V$ , which shows that the heavier particles freeze-out early.

(e) The effective temperature ( $T$ ), initial temperature ( $T_i$ ), kinetic freeze-out temperature ( $T_0$ ), mean  $\langle p_T \rangle$  and kinetic freeze-out volume ( $V$ ) are observed to be larger in central collisions and they decrease from central to periphery.

(f) The initial temperature is larger than the effective temperature, and the effective temperature larger than the kinetic freeze-out temperature. The chemical freeze-out temperature ( $T_{ch}$ ) lie between the initial and effective temperatures, and is nearly equal to the effective temperature and this sequence agrees the order of time evolution of the interacting system, even though both the effective and kinetic freeze-out temperatures are extracted at the kinetic freeze-out.

### Data availability

The data used to support the findings of this study are included within the article and are cited at relevant places within the text as references.

### Compliance with Ethical Standards

The authors declare that they are in compliance with ethical standards regarding the content of this paper.

### Funding

This research was funded by the National Natural Science Foundation of China grant number 11875052, 11575190, and 11135011, and Ajman University Internal Research grant number DGSR Ref. 2021-IRG-HBS-12, H.E.C Pakistan N.R.P.U Project Number 15785.

### Acknowledgements

We acknowledge the facilities provided by the University of Chinese Academy of Sciences China, Abdul Wali Khan University Mardan, Ajman University Ajman U.A.E and Ghazi University D. G Khan for carrying out the research.

## References

- [1] A. Andronic, P. Braun-Munzinger, J. Stachel, Nucl. Phys. A 772 (2006) 167.
- [2] J. Cleymans, H. Oeschler, K. Redlich, S. Wheaton, Phys. Rev. C 73 (2006) 034905.
- [3] A. Andronic, P. Braun-Munzinger, J. Stachel, Acta Phys. Pol. B 40 (2009) 1005.
- [4] A. Andronic, P. Braun-Munzinger, J. Stachel, Nucl. Phys. A 834 (2010) 237c.
- [5] J. Adams et al. (STAR Collaboration), Nucl. Phys. A 757 (2005) 102.
- [6] L. Adamczyk. et al., (STAR Collaboration), Phys. Rev. C 96 (2017) 044904.
- [7] S. Wheaton, J. Cleymans and M. Hauer, Comput. Phys. Commun. 180 (2009) 84.
- [8] A. Andronic, F. Beutler, P. Braun-Munzinger, et al., Phys. Lett. B 657 (2009) 312.
- [9] B. Abelev et al., (STAR Collaboration), Phys. Rev. C 79 (2009) 034909.
- [10] E. Schnedermann, J. Sollfrank, U. Heinz, Phys. Rev. C 48 (1993) 2462.
- [11] Q. Wang, F. H. Liu and K. K. Olimov, [arXiv: 2104.14271].
- [12] L. L. Li, F. H. Liu and Olimov, Entropy 23 (2021) 478. doi:10.3390/e23040478. [arXiv:2006.15333].
- [13] M. Waqas, F. H. Liu, Z. Wazir, Adv. High. Energy Phys. 2020 (2020) 8198126.
- [14] STAR Collaboration (B.I. Abelev et al.), Phys. Rev. C 81 (2010) 024911.
- [15] Z.B. Tang, Y.C. Xu, L.J. Ruan, G. van Buren, F.Q. Wang, Z.B. Xu, Phys. Rev. C 79 (2009) 051901(R).
- [16] H.R. Wei, F.H. Liu, R.A. Lacey, J. Phys. G 43 (2016) 125102.
- [17] P. P. Yang, M. Y. Duan and F. H Liu, Eur. Phys. J. A 57 (2021) 63. doi:10.1140/epja/s10050-021-00380-4. [arXiv:2012.10228[hep-ph]].
- [18] L. N. Gao, F. H. Liu and R. A. Lacey, Eur. Phys. J. A 52 (2016) 137. doi:10.1140/epja/i2016-1637-7. [arXiv:1604.07218 [hep-ph]].
- [19] D. H. E. Gross, Phys. Rept. **279** (1997) 119-201. doi:10.1016/S0370-1573(96)00024-5
- [20] B. Borderie, Journal of Physics G, vol. 28 (2002) R217 CR247 .
- [21] M. D Agostino, F. Gulminelli, Ph. Chomaz, M. Bruno, F. Cannata, R. Bougault, N. Colonna, F. Gramegna, I. Iori, N. Le Neindre, G. V. Margagliotti, P. F. Mastinu, P. M. Milazzo, A. Moroni, and G.Vannini, Physics Letters B, vol. 473 (2000) 219~C225.
- [22] M. D Agostino, R. Bougault, F. Gulminelli, M. Bruno, F. Cannata, Ph. Chomaz, F. Gramegna, I. Iori, N. Le Neindre, G. V. Margagliotti, A. Moroni, and G. Vannini, Nuclear Physics A, vol. 699 (2002) 795 C818.
- [23] P. Chomaz, V. Duflot, and F. Gulminelli, Physical Review Letters, vol. 85 (2000) 3587 C3590.
- [24] Y. Aoki, G. Endrodi, Z. Fodor, S.D. Katz, K.K. Szabo, Nature 443 (2006) 675.
- [25] M. Cheng, N.H. Christ, S. Datta, J. van der Heide, C. Jung, F. Karsch, O. Kaczmarek, E. Laermann, R.D. Mawhinney, C. Miao, P. Petreczky, K. Petrov, C. Schmidt, W. Soeldner, T. Umeda, Phys. Rev. D 77, (2008) 014511.

- [26] A. Barducci, R. Casalbuoni, S. De Curtis, R. Gatto, G. Pettini, Phys. Rev. D **41** (1990) 1610.
- [27] M. Asakawa, K. Yazaki, Nucl. Phys. A **504** (1989) 668.
- [28] M.A. Stephanov, Int. J. Mod. Phys. A **20** (2005) 4387.
- [29] M. A. Stephanov, Prog. Theor. Phys. Suppl. **153** (2004) 139.
- [30] Z. Fodor, S.D. Katz, JHEP **0404** (2004) 050.
- [31] R.V. Gavai, S. Gupta, Phys. Rev. D **78** (2008) 114503.
- [32] B. Povh, K. Rith, C. Soltz et al. Particle and nuclei, springer-verlag 2004.
- [33] R. Hagedorn, Riv. Nuovo Cimento **6**(10) (1983) 1.
- [34] G. Kadam, H. Mishra and M. Panero, [arXiv:2011.02171 [hep-ph]].
- [35] R. Rath, A. Khuntia, R. Sahoo and J. Cleymans, J. Phys. G **47** (2020) 055111. doi:10.1088/1361-6471/ab783b [arXiv:1908.04208 [hep-ph]].
- [36] L. L. Li and F. H. Liu, Eur. Phys. J. A **54** **10**, (2018) 169. doi:10.3847/1538-4365/aada4a [arXiv:1809.03881 [hep-ph]].
- [37] M.Waqas and B.C.Li, "Adv.High Energy Phys. 2020 (2020) 1787183.
- [38] G.G. Barnaf?ldi, K. urm?ssy, T.S. Biro, J. Phys. Conf. Ser. **270** (2011) 012008.
- [39] J.C. Chen, Z.P. Zhang, G.Z. Su, L.X. Chen, Y.G. Shu, Phys. Lett. A **300** (2002) 65.
- [40] J.M. Conroy, H.G. Miller, Phys. Rev. D **78** (2008) 054010.
- [41] G. Biro. G.G. Barnaf?ldi, T.S. Biro, K. urm?ssy, AIP Conf. Proc. **1853** (2017) 080001.
- [42] A.M. Teweldeberhan, A.R. Plastino, H.G. Miller, Phys. Lett. A **343** (2004) 71.
- [43] J. Cleymans and M. W. Parada, MDPI Physics **2** (2020) 654-664. doi:10.3390/physics2040038
- [44] P. Pareek and S. K. Tiwari, J. Phys. Conf. Ser. **1690** (2020) 012136. doi:10.1088/1742-6596/1690/1/012136
- [45] Z. Ramezani and A. Pourdarvish, Physica A **561** (2021) 125273. doi:10.1016/j.physa.2020.125273
- [46] M. Waqas, F. H. Liu and Z. Wazir, Adv. High Energy Phys. **2020** (2020) 8198126. doi:10.1155/2020/8198126 [arXiv:2004.03773 [hep-ph]].
- [47] M. Waqas, F. H. Liu, L. L. Li and H. M. Alfanda, Nucl. Sci. Tech. **31** (2020) 109. doi:10.1007/s41365-020-00821-7 [arXiv:2001.06796 [hep-ph]].
- [48] R. Odorico, Phys. Lett. B **118** (1982) 151.
- [49] ALICE Collaboration (K. Aamodt et al.), Phys. Lett. B **693** (2010) 53.
- [50] T. Mizoguchi, M. Biyajima, N. Suzuki, Int. J. Mod. Phys. A **32** (2017) 1750057.
- [51] UA1 Collaboration (G. Arnison et al.), Phys. Lett. B **118** (1982) 167.
- [52] L. Adamczyk et al. [STAR], Phys. Rev. C **96** (2017) no.4, 044904 doi:10.1103/PhysRevC.96.044904 [arXiv:1701.07065 [nucl-ex]]
- [53] S. S. Adler et al. [PHENIX], Phys. Rev. C **69** (2004), 034909 doi:10.1103/PhysRevC.69.034909 [arXiv:nucl-ex/0307022 [nucl-ex]].
- [54] J. Adam et al. [STAR], Phys. Rev. C **99** (2019) 064905. doi:10.1103/PhysRevC.99.064905 [arXiv:1903.11778 [nucl-ex]].
- [55] D. Zhang [STAR], Nucl. Phys. A. **1005** 2021 121825. doi:10.1016/j.nuclphysa.2020.121825
- [56] D. Thakur, S. Tripathy, P. Garg, R. Sahoo and J. Cleymans, "Indication of a Differential Freeze-out in Proton-Proton and Heavy-Ion Collisions at RHIC and LHC energies," Adv. High Energy Phys. **2016**, 4149352 (2016) doi:10.1155/2016/4149352 [arXiv:1601.05223 [hep-ph]]
- [57] D. Thakur, S. Tripathy, P. Garg, R. Sahoo and J. Cleymans, "Indication of Differential Kinetic Freeze-out at RHIC and LHC Energies," Acta Phys. Polon. Supp. **9**, 329 (2016) doi:10.5506/APhysPolBSupp.9.329 [arXiv:1603.04971 [hep-ph]]
- [58] L J Gutay, A S Hirsch, R P Scharenberg, B K Srivastava and C Pajares Int. J. Mod. Phys. E **24** (2015) 1550101.
- [59] A S Hirsch, C Pajares, R P Scharenberg and B K Srivastava Phys. Rev. D **100** (2019) 114040.
- [60] P Sahoo, S De, S K Tiwari and R Sahoo Eur. Phys. J. A **54** (2018) 136.
- [61] D Thakur, S Tripathy, P Garg, R Sahoo and J Cleymans Adv. High Energy Phys. **2016** (2016) 4149352.
- [62] I Melo and B Tomasik J. Phys. G **43** (2016) 015102.
- [63] M. Waqas and G. X. Peng, Adv. High Energy Phys. **2021** (2021), 6674470 doi:10.1155/2021/6674470 [arXiv:2103.07852 [hep-ph]]
- [64] M. Waqas, F. H. Liu, R. Q. Wang and I. Siddique, Eur. Phys. J. A **56** (2020) no.7, 188 doi:10.1140/epja/s10050-020-00192-y [arXiv:2007.00825 [hep-ph]]
- [65] M. Waqas, G. X. Peng, F. H. Liu and Z. Wazir, Sci. Rep. **11** (2021) no.1, 20252 doi:10.1038/s41598-021-99455-x [arXiv:2105.01300 [hep-ph]]
- [66] F.-H. Liu, Y.-Q. Gao, T. Tian, and B.-C. Li, The European Physical Journal A, vol. 50 (2014) 94.
- [67] W.-J. Xie, j<sup>o</sup> Chinese Physics C, vol. 35 (2011) 1111~C 1119.
- [68] J.-Y. Ollitrault, j<sup>o</sup>Revealing QCD thermodynamics in ultra-relativistic nuclear collisions,j<sup>±</sup> Proc. 28th Int. Conf. Ultrarelativistic Nucleus-Nucleus Collisions (Quark Matter 2019), Wuhan, China, 4~C9 Nov. 2019, Nuclear Physics A, to appear, 2020